Array Processing Underground

J H McClellan

School of Electrical and Computer Engineering
Georgia Institute of Technology
Atlanta, GA 30332

25 June 2014

Millions of Landmines

Minehunting with radar and rats

DURING a morning operation against the Taliban in Afghanistan's Helmand province in 2010, a British army contingent halted before a narrow pass reckoned to be mined with improvised explosive devices (IEDs). The day before, two of the unit's armoured vehicles had been destroyed nearby by IEDs (the crews were uninjured). The commander, Lieutenant-Colonel Matt Bazeley, fired a rocket that pulled 200 metres of a fat, coiled hose out over the route ahead. Packed with about 1.5 tonnes of explosives, it detonated upon landing with

Clearing landmines: Despite sophisticated new technology many explosive devices are still cleared by hand with the help of trained animals

clearing mines manually.

Humanitarian demining, as post-conflict mine clearance is known, is carried out by the army, non-governmental organisations (NGOs) and commercial companies.

plastic. They might contain only one metal component: a firing pin smaller than a sewing needle, says Eddie Banks, a retired deminer and author of a book on landmine design. But some hand-held detectors are sensitive enough to detect even a buried scrap of silvery paper from a cigarette pack, says Alex van Roy of the Armenian government's Centre for Humanitarian Demining and Expertise, a new body clearing mines in Armenia that remain after a war in the 1990s with Azerbaijan.

Such machines cost about $4,000 and

Thanks

- Prof. Waymond Scott
- Dr. Mubashir Alam
- Dr. Ali Cafer Gurbuz
- Dr. Mu-Hsin Wei
- Dr. Kyle Krueger
- Dr. Michael Oristaglio
- Mr. Hadi Jamli-Rad

Ideal Fan Filter

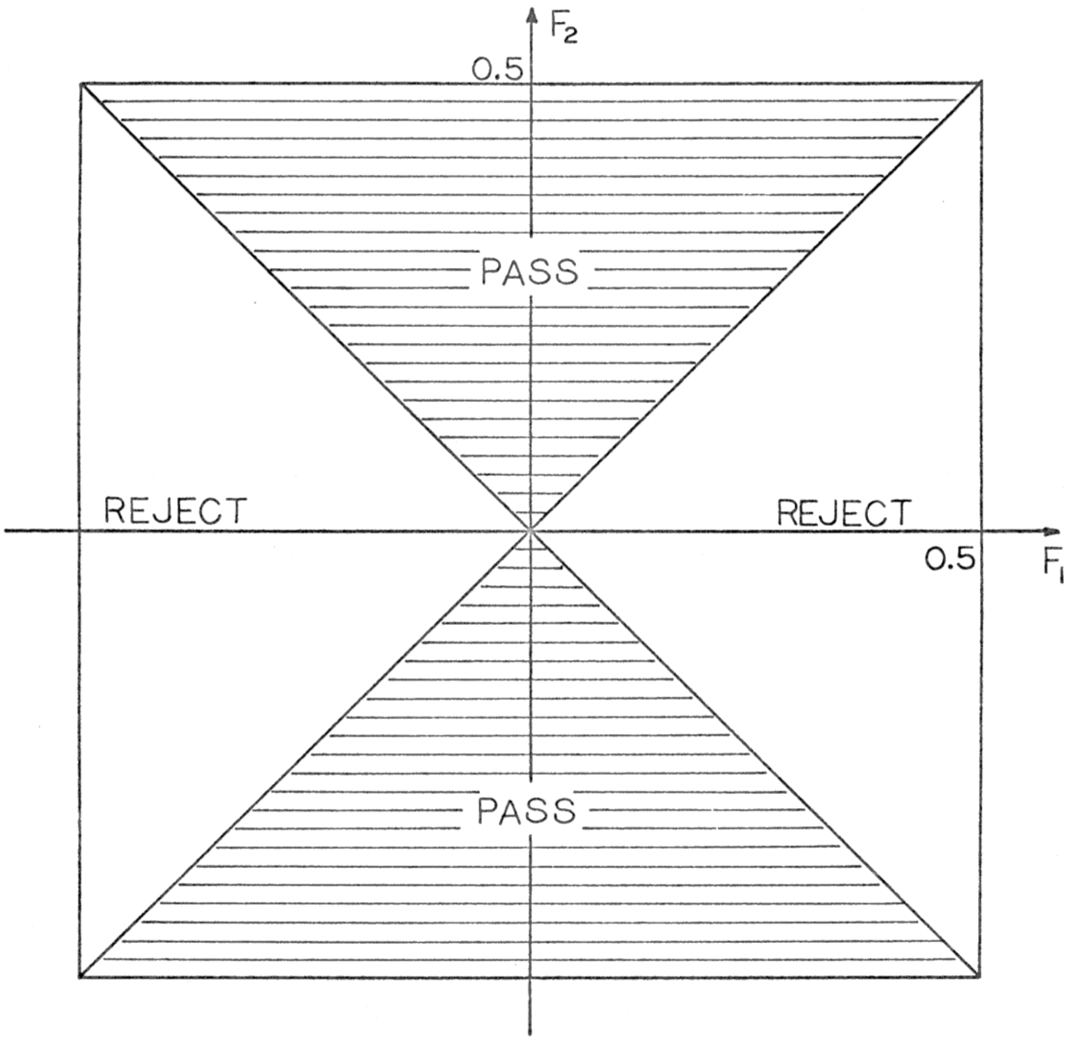

John Shanks
Sven Treitel
AMOCO

f-k Filtering

2-D SPECTRUM ANALYSIS

- FREQUENCY-WAVENUMBER SPECTRUM DISPLAYS WAVES

$$s(x,t) \quad \longleftrightarrow \quad S(k,f) \quad \text{or} \quad S(k,\omega)$$

"f-k" SPECTRUM

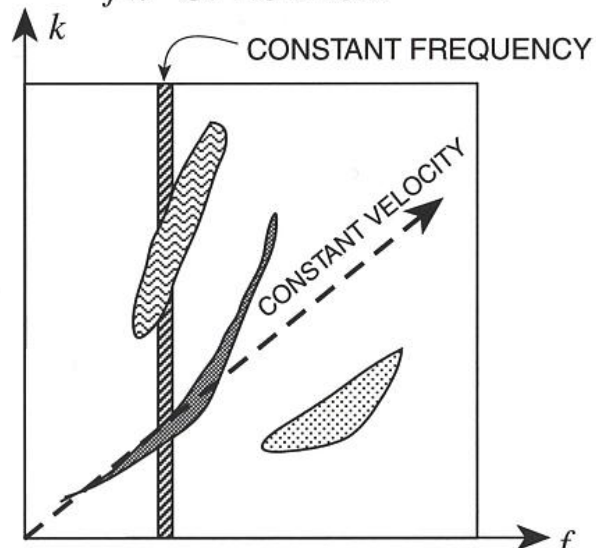

AT A CONSTANT FREQUENCY
THERE ARE VERY DISTINCT PEAKS

Sample in Space with an Array of Sensors and in Time

1-D to 2-D Transformation

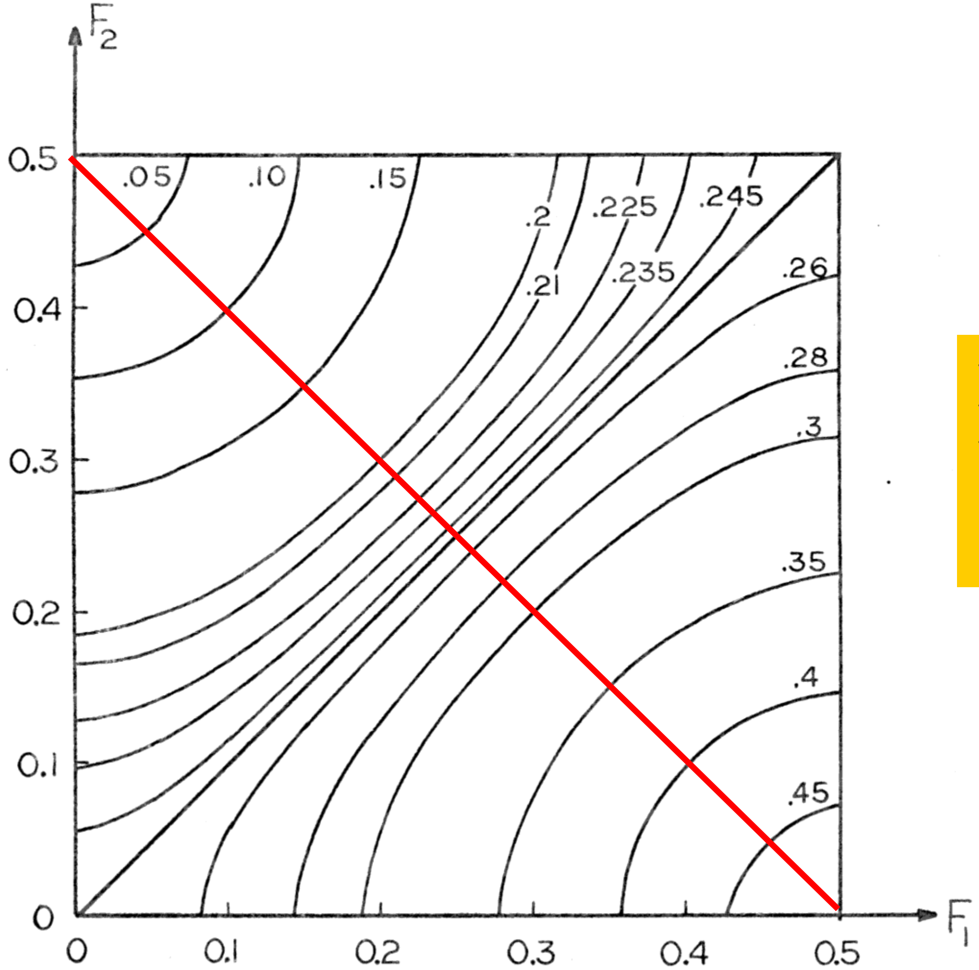

Make 2-D FIR Filters
From 1-D FIR Filters
(Optimal Equiripple)

Actual 2-D Frequency Response

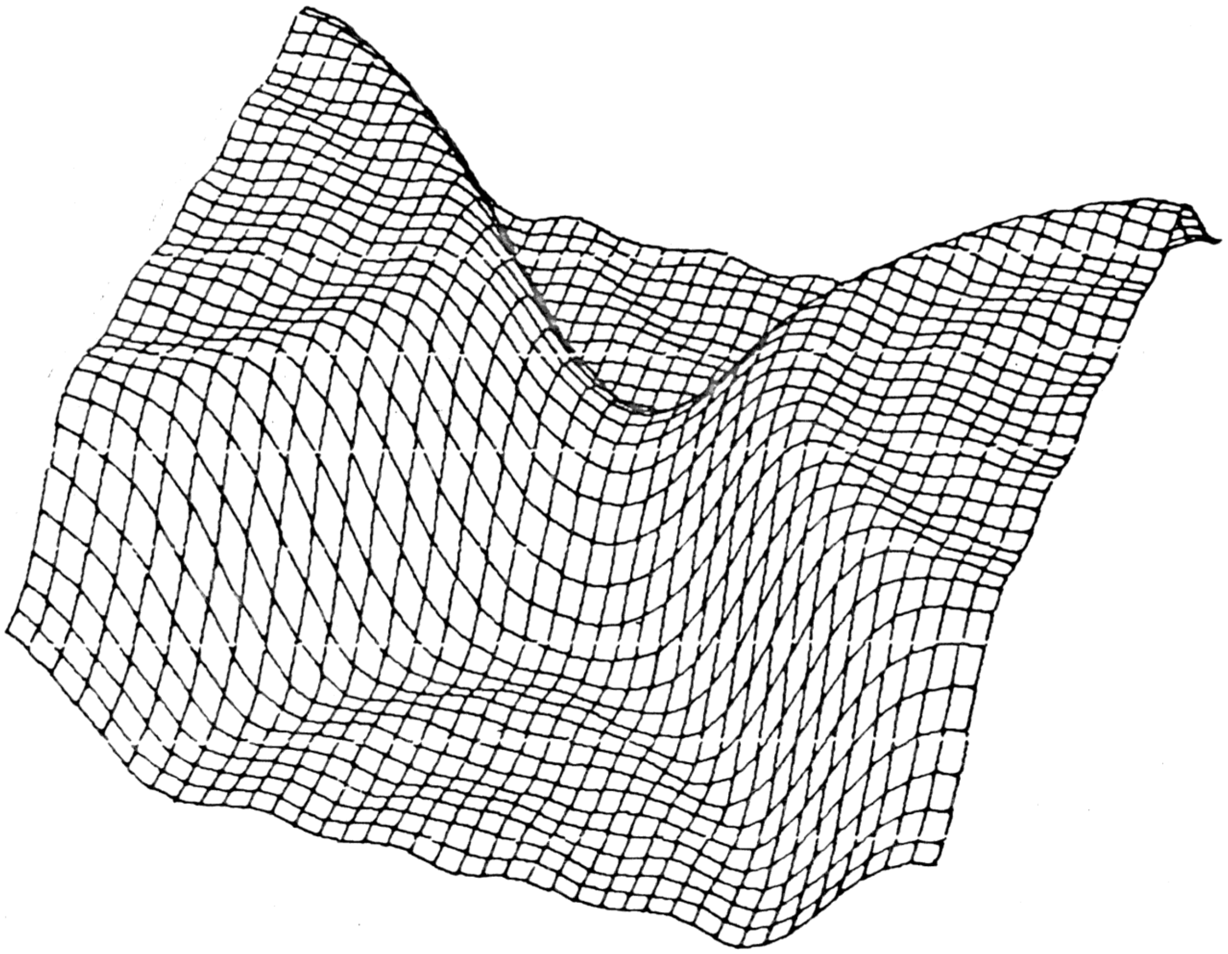

Well Logging (1980's)

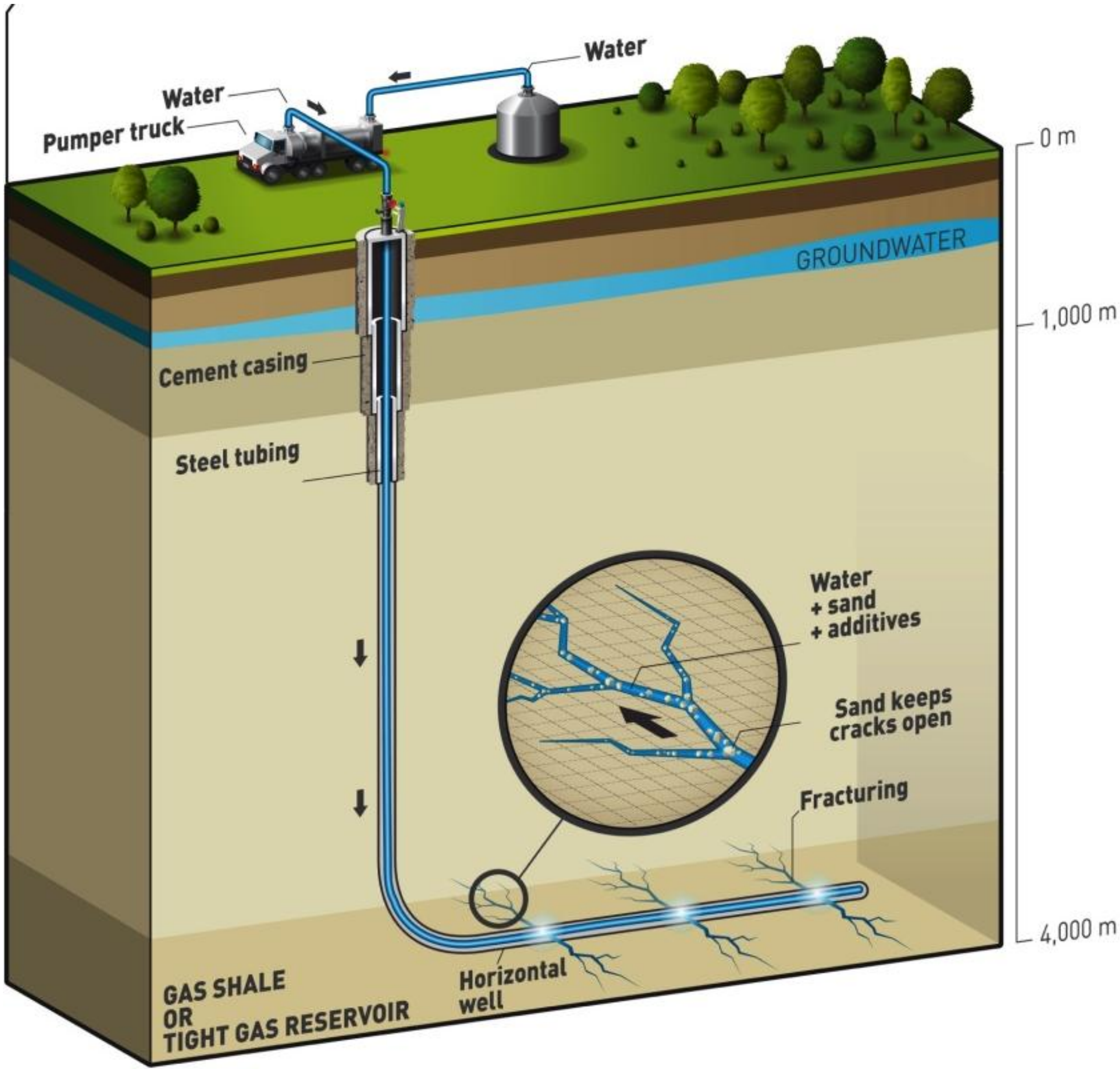

Acoustic Dispersion Curves

WELL-LOGGING EXAMPLE

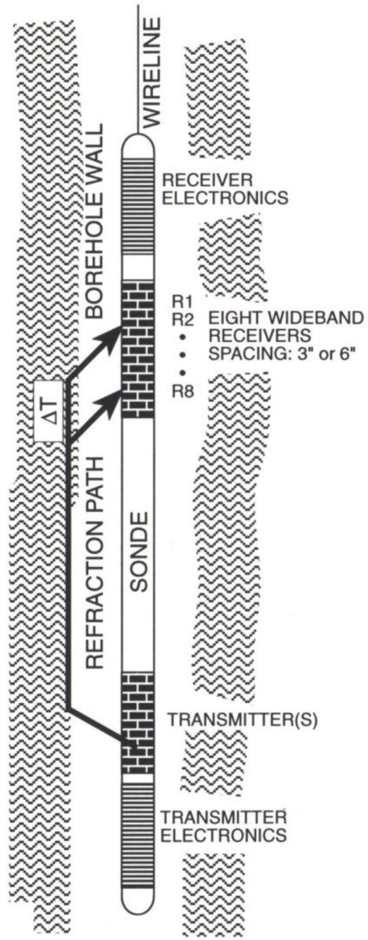

- $s(z,t)$ is SUITE of RECORDED PRESSURE WFMS
- WAVE PHYSICS:

$$S(z,\omega) = X(\omega)\int A(k,\omega)e^{-jkz}dk$$

$\Longrightarrow$ $A(k,\omega)$ is FREQ-WAVENUMBER RESPONSE of ROCK FORMATION

- SOLUTION IN TERMS OF SINGULARITIES

$$S(z,\omega) = \sum\{\text{residues(poles)}\} + \int\{\text{branch-cuts}\}$$

- RESIDUES $\Longrightarrow$ PROPAGATING MODES
- BRANCH-CUTS $\Longrightarrow$ BODY WAVES

$\Longrightarrow$ THEREFORE, LOOK FOR POLES/PEAKS in $A(k,\omega)$

12-channel Sonic Tool

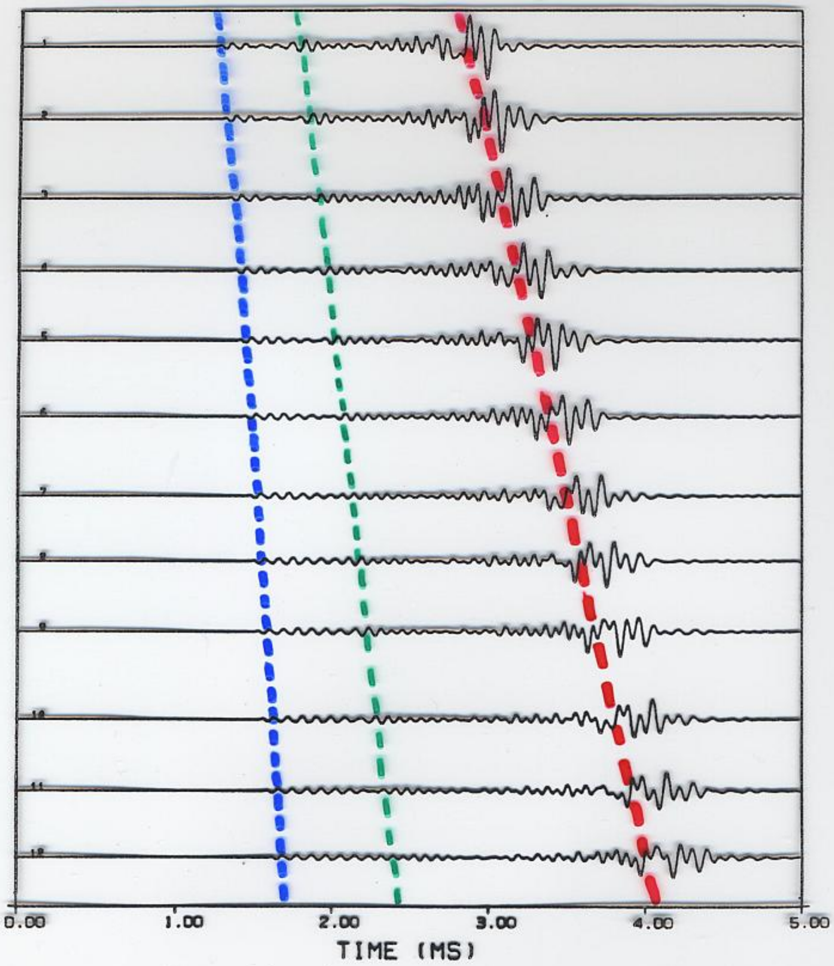

Fig. 2. TYPICAL RECEIVED SIGNALS. Casing arrival at 57 μsec/ft. dominates the early part of the waveform. Formation compressional slowness = 70 μsec/ft., shear slowness = 138 μsec/ft, sampling rate = 100 kHz, spatial separation = 6 inches.

Exponential Model vs. space

PRONY WORKS FOR WIDEBAND ARRAYS

- COMPUTE DFT OF EACH CHANNEL:

$$S(\ell, f) = \text{FFT}\{s(\ell, t)\} \qquad \text{(FFT versus } t\text{)}$$

- AT EACH FREQ, DETERMINE $\boxed{\text{EXPONENTIAL}}$ MODEL: (NARROWBAND)

$$S(\ell, f) \approx \sum_{i=1}^{P} G_i(f) e^{-(\alpha_i + j2\pi f p_i)\ell} \qquad \ell = 0, 1, 2, \ldots, L-1$$

p_i is slowness, f is frequency

- RECEIVER INDEX is DENOTED by ℓ

Dispersion: velocity vs. freq

RELATING ROOTS TO SLOWNESS

- ROOTS of LINEAR PREDICTION POLYNOMIAL $A(z)$
  GIVE SINUSOIDAL FREQUENCIES

- FOR THE ARRAY CASE, a PURE SINUSOID vs. DISTANCE (ℓ)

$$s[\ell] \approx \sum_i G_i \, e^{j\omega_i \ell}$$

WHERE ℓ IS SAMPLE INDEX vs. SPACE; AND "ω_i" IS SPATIAL FREQ

- EACH ROOT of $A(z)$ is z_i (COMPLEX-VALUED)

$$z_i = e^{(\alpha_i + j2\pi f p_i)} \qquad \Longrightarrow \qquad p_i = \frac{\angle z_i}{2\pi f}$$

- "SLOWNESS" of i^{th} WAVE (p_i) VARIES vs. f

$\Longrightarrow$ $p_i(f)$ IS "DISPERSION RELATION"

12-channel Sonic Tool

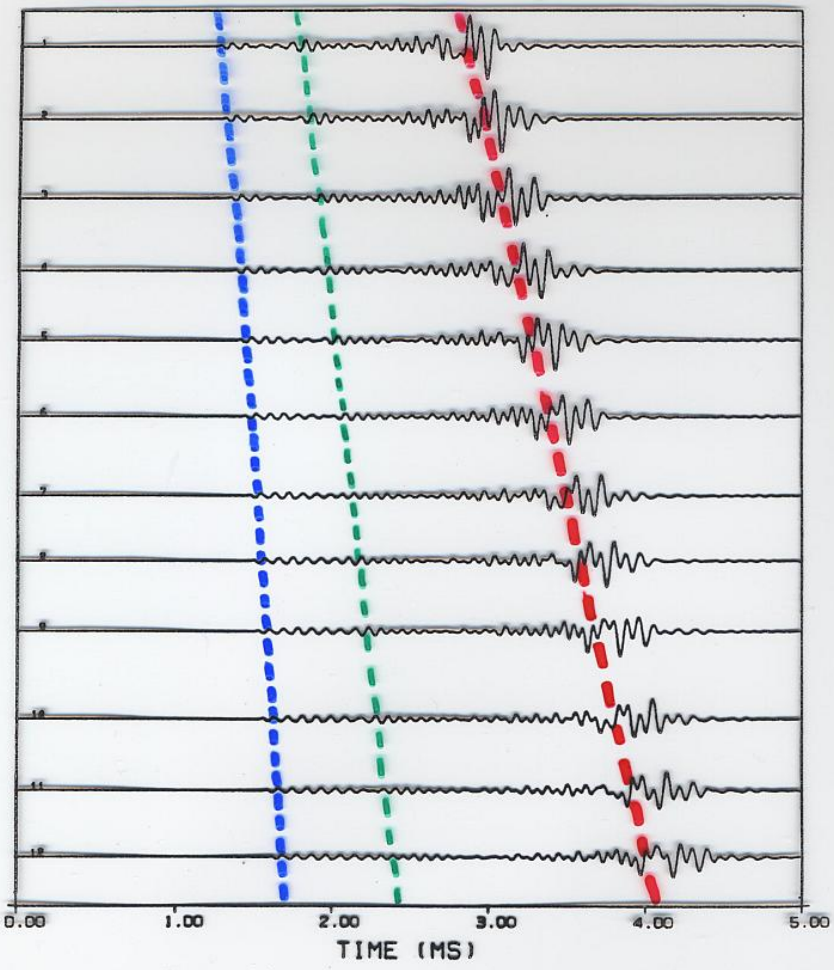

Fig. 2. TYPICAL RECEIVED SIGNALS. Casing arrival at 57 μsec/ft. dominates the early part of the waveform. Formation compressional slowness = 70 μsec/ft., shear slowness = 138 μsec/ft, sampling rate = 100 kHz, spatial separation = 6 inches.

“Sparse” freq-space spectrum

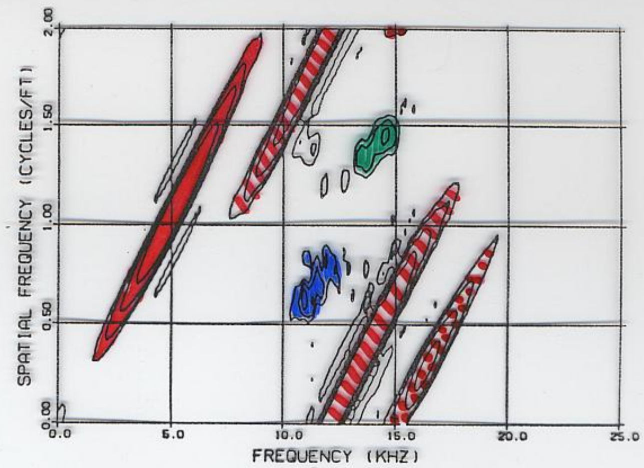

Fig. 4. CONTOUR PLOT OF FOURIER SPECTRUM. Only frequencies from 0 to 25 kHz are shown since the effective bandwidth of the signals is about 20 kHz.

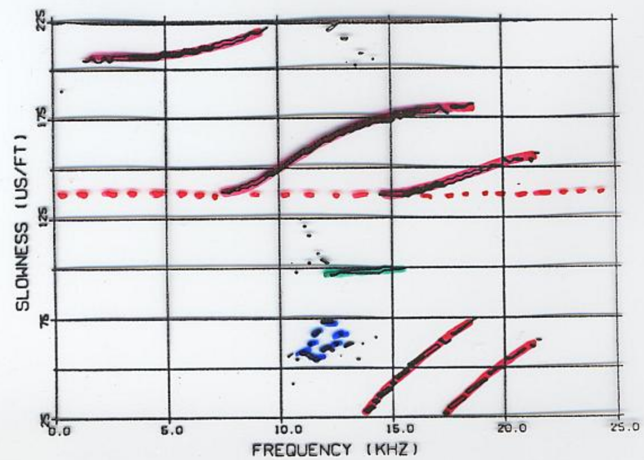

Fig. 7. SLOWNESS-FREQUENCY PLOT FROM PRONY ROOTS. Slowness from 5 roots of Prony model computed at each frequency. Magnitude of complex amplitude factor from Prony model is plotted on a log scale.

Plot slowness vs frequency

$p_i = k/f$ vs. f

“Sparsity” Dispersion curves

SPARSITY PENALIZED RECONSTRUCTION FRAMEWORK FOR BROADBAND DISPERSION EXTRACTION

Shuchin Aeron, Sandip Bose and Henri-Pierre Valero

Schlumberger-Doll Research, Cambridge, MA

Venkatesh Saligrama

Boston University, Boston, MA

ICASSP-2010

$$s(l,t) = \int_0^\infty \sum_{m=1}^{M(f)} S_m(f) e^{-(i2\pi k_m(f))z_l} e^{i2\pi f t} df \qquad (3)$$

where $S_m(f) = S(f)q_m(f)$ and the approximation error is absorbed in the noise. Under this model, the data acquired across the receivers can be written in the frequency domain as,

$$\underbrace{\begin{bmatrix} Y_1(f) \\ Y_2(f) \\ \vdots \\ \vdots \\ Y_L(f) \end{bmatrix}}_{\mathbf{Y}(f)} = [\mathbf{v}_1(f), ..., \mathbf{v}_M(f)] \underbrace{\begin{bmatrix} S_1(f) \\ S_2(f) \\ \vdots \\ \vdots \\ S_M(f) \end{bmatrix}}_{\mathbf{S}(f)} + \underbrace{\begin{bmatrix} W_1(f) \\ W_2(f) \\ \vdots \\ \vdots \\ W_L(f) \end{bmatrix}}_{\mathbf{W}(f)} \qquad (4)$$

where $\mathbf{v}_i(f) = [e^{-i2\pi k_i(f)z_1}, ..., e^{-i2\pi k_i(f)z_L}]^T$ and $Y_l(f), S_l(f)$ and $W_l(f)$ denote the Discrete Fourier Transforms of $y((l,t), s(l,t)$ and $w(l,t)$ respectively. In other words the data at each frequency is a superposition of $M(f)$ exponentials sampled at the receiver locations $z_1, .., z_L$.

Model that can be enumerated

Schlumberger-2010 (2)

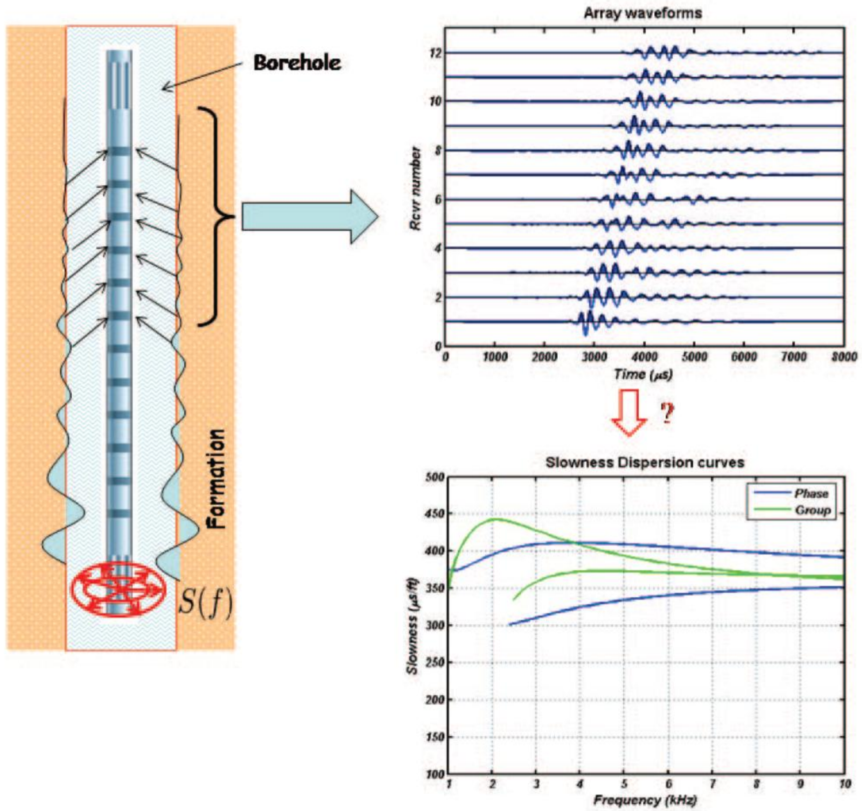

Fig. 1. Schematic showing the generation and acquisition of acoustic waves by the sonic tool in a fluid filled borehole on the left. The corresponding dispersion extraction problem consists in using the array waveform traces collected at one depth as shown on the top right to estimate the dispersion curves shown on the bottom right.

Schlumberger-2010 (3)

dispersion curve is parameterized by its phase and group slowness. This is depicted in Fig. 2(a). Without loss of generality we assume that the number of modes $M(f)$ is the same for all frequencies in the band of interest. For the sake of brevity we denote this number by M. Under the linear approximation of the dispersion curve(s) for the modes, the sampled exponential at a frequency f corresponding to a mode can be written in a parametric form as

$$\mathbf{v}_m(f) = \begin{bmatrix} e^{-i2\pi(k_m + k_m^{'}(f-f_0))z_1} \\ e^{-i2\pi(k_m + k_m^{'}(f-f_0))z_2} \\ \vdots \\ e^{-i2\pi(k_m + k_m^{'}(f-f_0))z_L} \end{bmatrix} \tag{6}$$

for $m = 1, 2, ..., M$ $f, f_0 \in \mathcal{F}$. Clearly, over the set of frequencies $f \in \mathcal{F}$, the collection of sampled exponentials (for a fixed m) $\{\mathbf{v}_m(f)\}_{f \in \mathcal{F}}$ as defined above corresponds to a line segment in the f-k domain thereby parameterizing the *wavenumber response* of the mode in the band in terms of phase and group slowness. In the following we will represent the band $\mathcal{F}$ by F which is a finite set of frequencies contained in $\mathcal{F}$,

$$F = \left\{ f_1, f_2, ..., f_{N_f} \right\} \subset \mathcal{F} : f_0 \in F \tag{7}$$

Schlumberger-2010 (4)

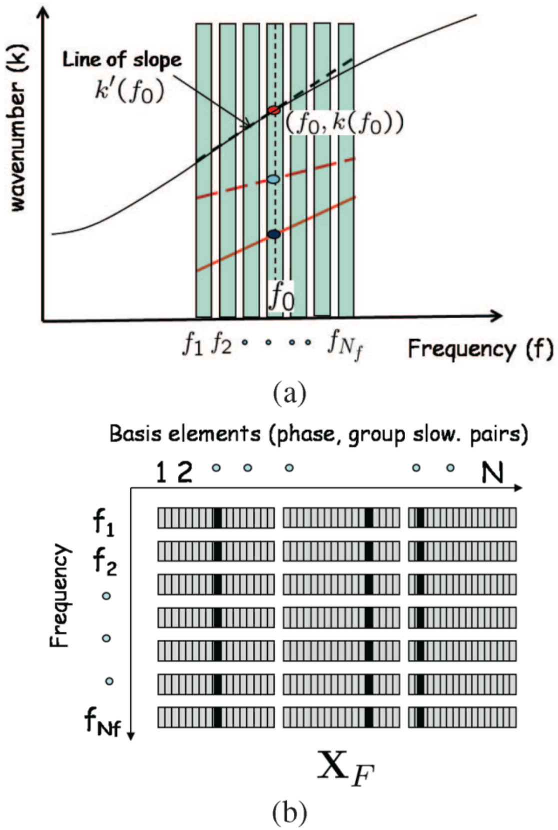

Fig. 2. Fig. 2(a) depicts the linearization of the dispersion curves in the f-k domain around f_0. Fig. 2(b) depicts column sparsity of the signal support in $\mathbf{\Phi}$ resulting from the sparsity in the number of modes in the given band.

Constraint is Group Sparsity (Joint Sparsity)

Schlumberger-2010 (5)

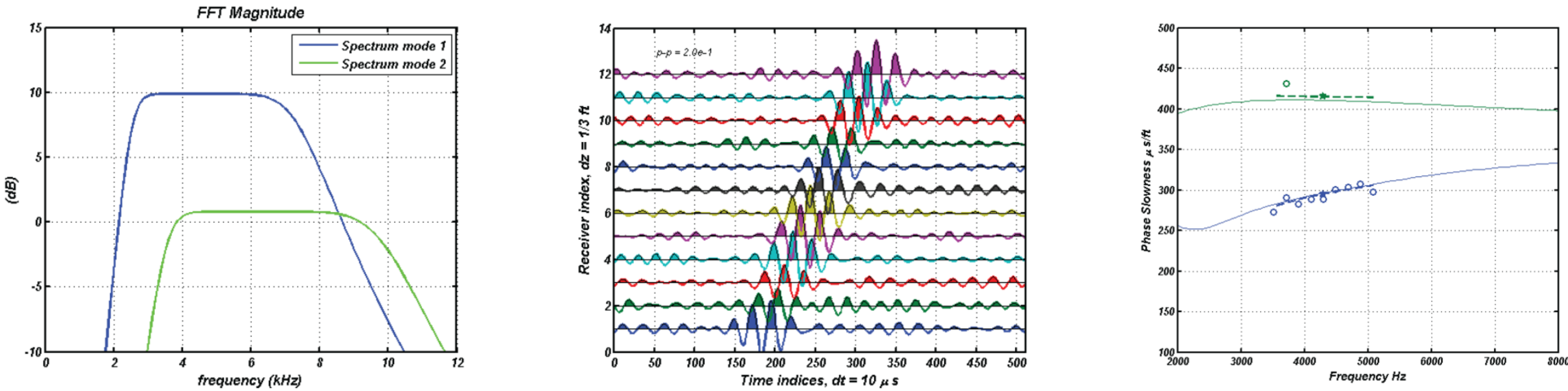

(a) (b) (c)

Fig. 3. (a) Figure showing the frequency spectrum of the modes. Note the frequency overlap. (b) Figure showing the data in the band 3.7 kHz - 5.2 kHz. Note the significant time overlap in the modes. (c) Dispersion Extraction results in the given band. The thin solid lines are the true dispersion curves for the two modes. The pentagrams are the estimates of the phase slowness at the center frequency of 4.5 kHz as obtained using the proposed method. The thick dashed lines are the corresponding estimated dispersion curves in the band. The blue and green circles are the dispersion curves obtained using the narrowband Matrix Pencil method of [3]. Note the superior performance of the proposed method over the Matrix Pencil based method.

Millions of Landmines

The Economist Technology Quarterly June 7th 2014 — Inside story 15

Minehunting with radar and rats

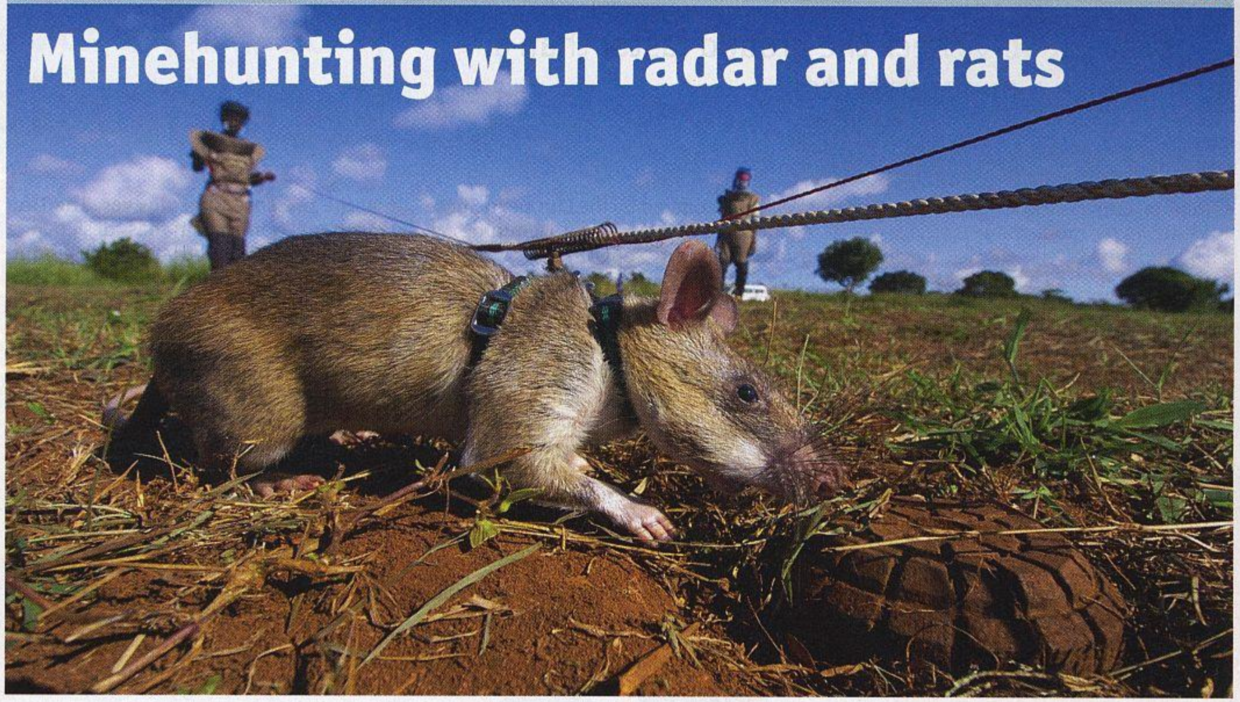

DURING a morning operation against the Taliban in Afghanistan's Helmand province in 2010, a British army contingent halted before a narrow pass reckoned to be mined with improvised explosive devices (IEDs). The day before, two of the unit's armoured vehicles had been destroyed nearby by IEDs (the crews were uninjured). The commander, Lieutenant-Colonel Matt Bazeley, fired a rocket that pulled 200 metres of a fat, coiled hose out over the route ahead. Packed with about 1.5 tonnes of explosives, it detonated upon landing with

Clearing landmines: **Despite sophisticated new technology many explosive devices are still cleared by hand with the help of trained animals**

clearing mines manually.

Humanitarian demining, as post-conflict mine clearance is known, is carried out by the army, non-governmental organisations (NGOs) and commercial companies.

plastic. They might contain only one metal component: a firing pin smaller than a sewing needle, says Eddie Banks, a retired deminer and author of a book on landmine design. But some hand-held detectors are sensitive enough to detect even a buried scrap of silvery paper from a cigarette pack, says Alex van Roy of the Armenian government's Centre for Humanitarian Demining and Expertise, a new body clearing mines in Armenia that remain after a war in the 1990s with Azerbaijan.

Such machines cost about $4,000 and

Detection of Subsurface Objects

- Why is important?
  - Buried Landmines and Improvised Explosive Devices are a Horrendous Problem
    - 100 million landmines buried throughout the world
    - 26,000 injuries and deaths per year
    - IEDs wound and kill as many soldiers as combat
  - Unexploded Ordinance
  - Tunnels
  - Utilities
  - Treasure

PSS-14

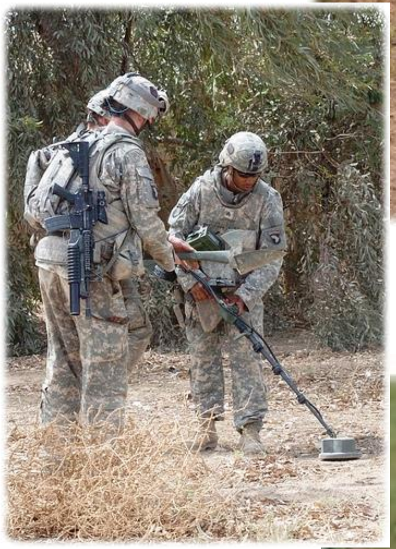

PSS-14

Autonomous Robotic System

Detection of Subsurface Objects

- Subsurface detection methodologies
  - Ground Penetrating Radar (GPR)
  - Seismic
  - Electromagnetic Induction (EMI)
  - Manual probing
  - Nuclear Quadrupole Resonance (NQR)
  - Biological
  - Infrared/Hyperspectral
  - Electrical Impedance Tomography
  - X-Ray Backscatter
  - Neutron Technologies
  - Electrochemical Methods

Detection of Subsurface Objects

- Given the success of medical imaging and terrestrial radars, finding buried objects would not seem to be difficult
- Robust methods for finding subsurface objects in general have proven to be very difficult
- **Why is it so difficult?**
  - **Cluttered environment**
    - **Inhomogeneous soil**
    - **False targets**
  - Only access to surface
    - Makes imaging very ill conditioned
  - Measurement time restrictions

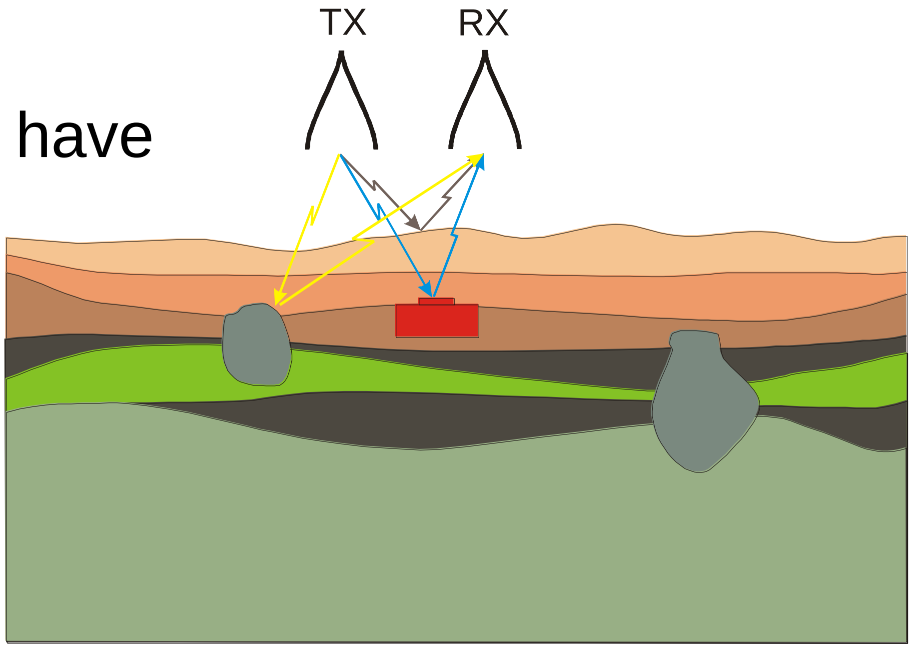

Drs. Waymond Scott & M. Alam

- **Spectrum Analysis of <u>Seismic</u> Surface Waves**
  - Separation of seismic waves
  - New Prony based spectrum analysis technique
    - Processing results and applications

- **Locating Buried Targets (landmines) by using <u>Seismic</u> Waves**
  - Waves separation and ID by vector-IQML
  - Imaging algorithm
    - Optimal maneuvering

Prototype Seismic Mine Detection System

Interaction of Rayleigh wave with mines can be used for detection and localization of mines

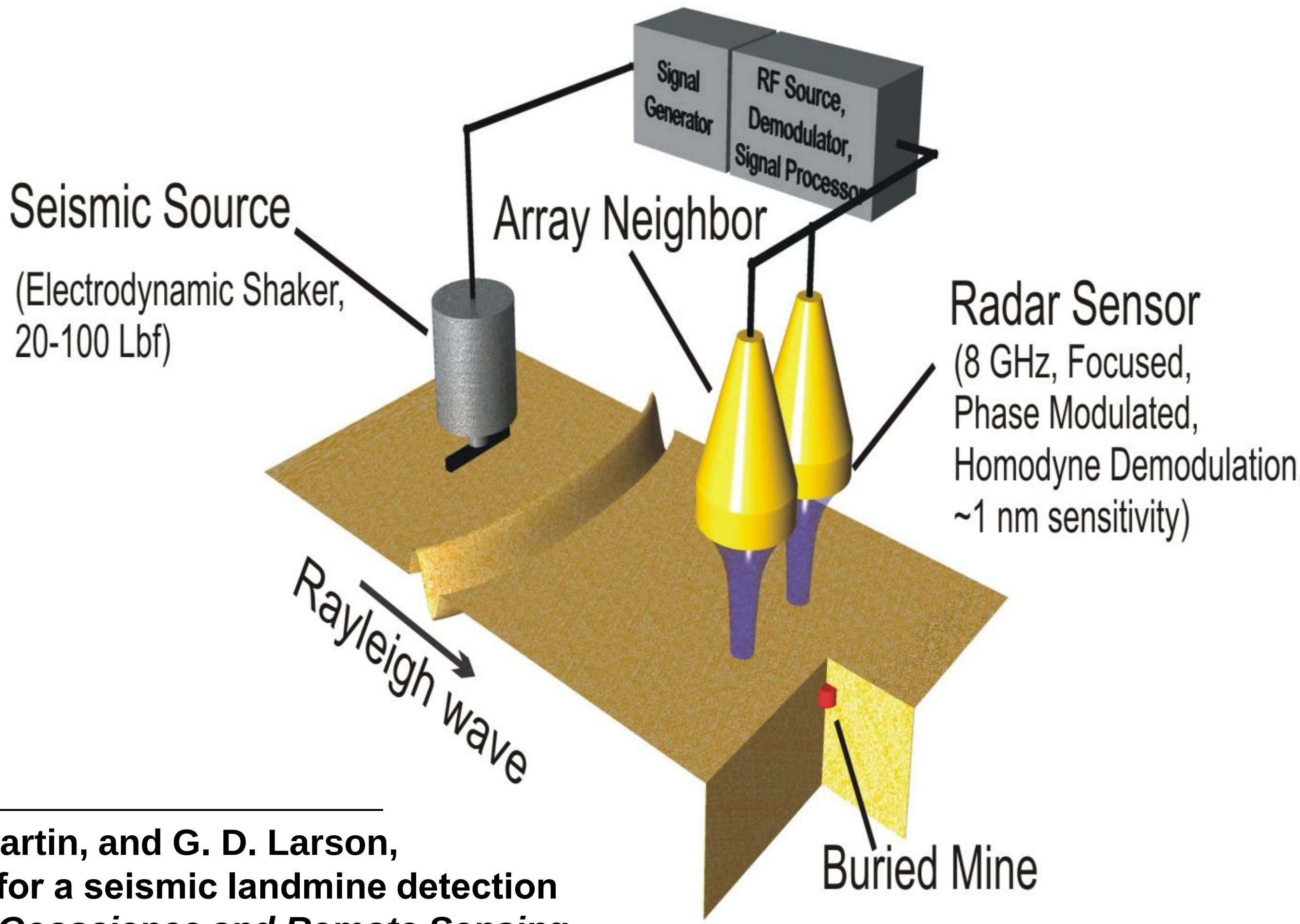

W. R. Scott Jr., J. S. Martin, and G. D. Larson, "Experimental model for a seismic landmine detection system," ***IEEE Trans. Geoscience and Remote Sensin*****g, vol. 39, pp. 1155–1164, June 2001.**

AP Mine: 1.3 cm deep

Raw Measured Data

Elastic Wave Sources and Sensors Development

Electrodynamic Shaker

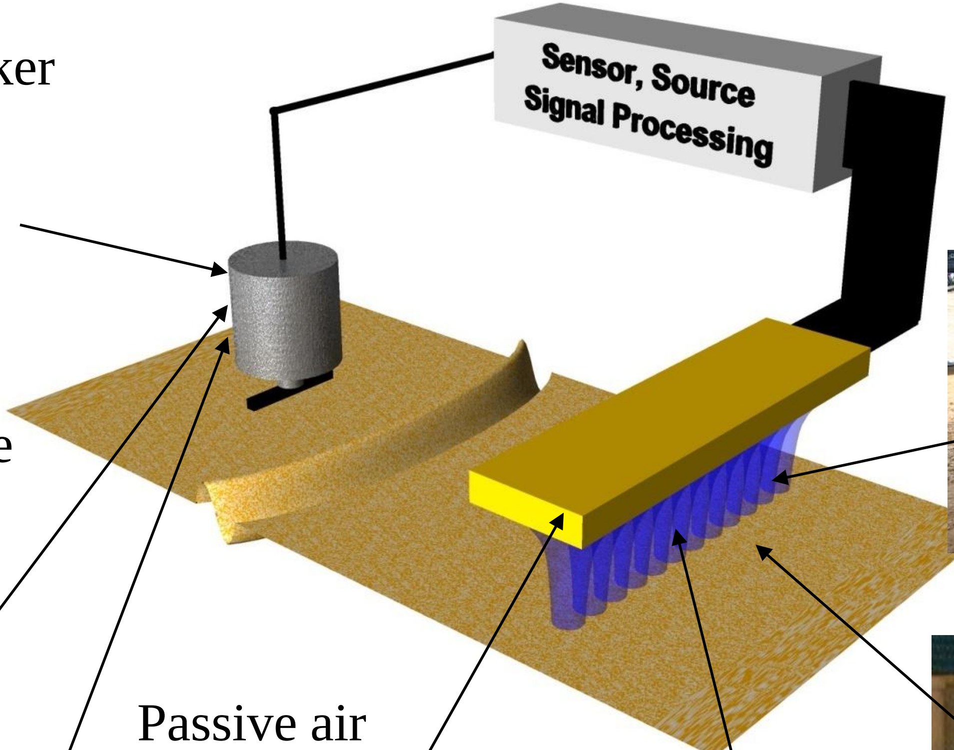

Ground Contacting Sensors

Air acoustic source

Radar Sensor

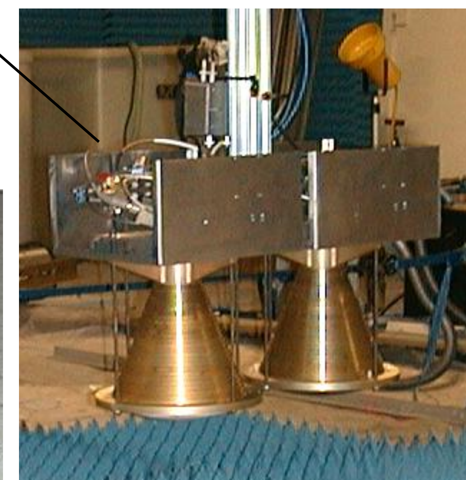

Electrical arc source

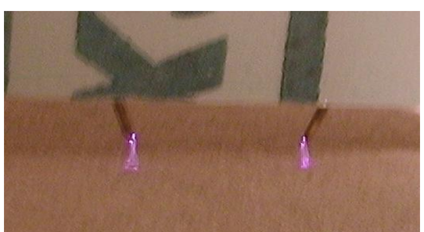

Passive air acoustic sensor

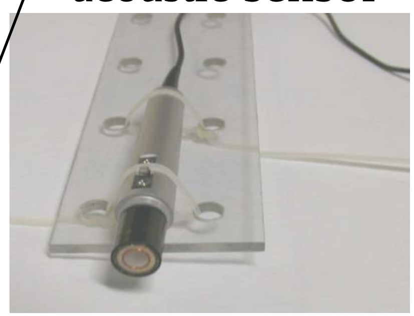

Ultrasonic sensor

Multi-Channel Extension

- Each channel can be modeled individually and then match them in the (k, ω) domain
- **Determine one model for two channels simultaneously**
  - **Same pole (k), different zeros (A)**
- Derive and use multi-channel IQML (multi-channel extension of Steiglitz-McBride)

$$\underline{\mathbf{S}}(x,\omega) = \begin{bmatrix} S_x(x,\omega) \\ S_z(x,\omega) \end{bmatrix}$$

$$\approx \begin{bmatrix} \sum_{p=1}^{P} A_{xp}(\omega) e^{j k_p(\omega) x} \\ \sum_{p=1}^{P} A_{zp}(\omega) e^{j k_p(\omega) x} \end{bmatrix}$$

Two Channel Space-Time Data

Numerical FDTD Data

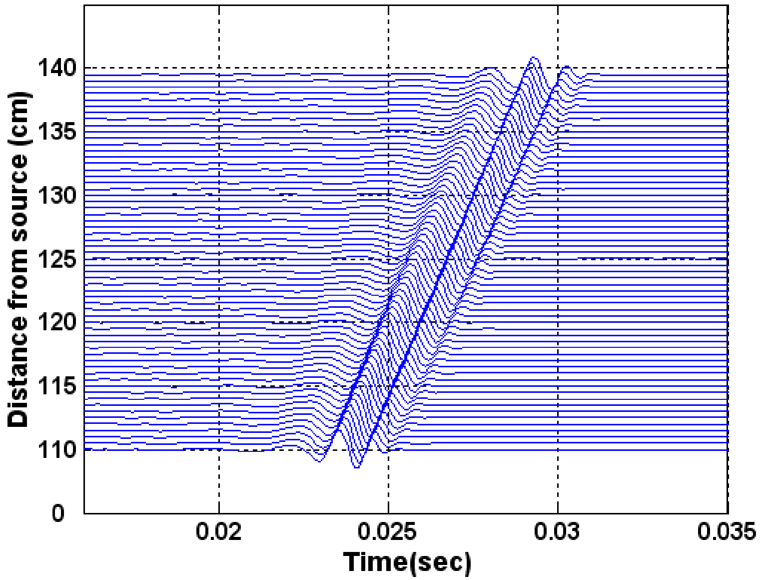

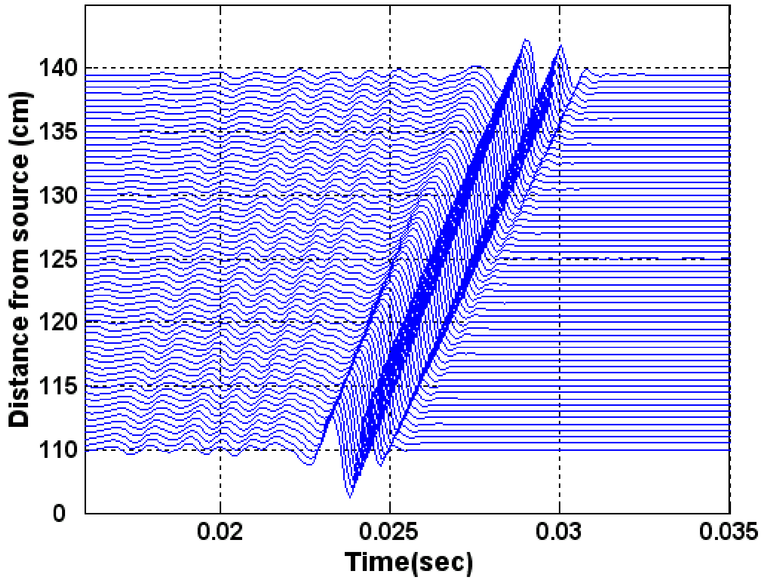

Channel-x

Channel-z

Spectrum Analysis and Polarization

Complex amplitude for “x” and “z” are used to create polarization ellipse at each (k , ω)

$$A_x \quad \text{vs.} \quad A_z$$

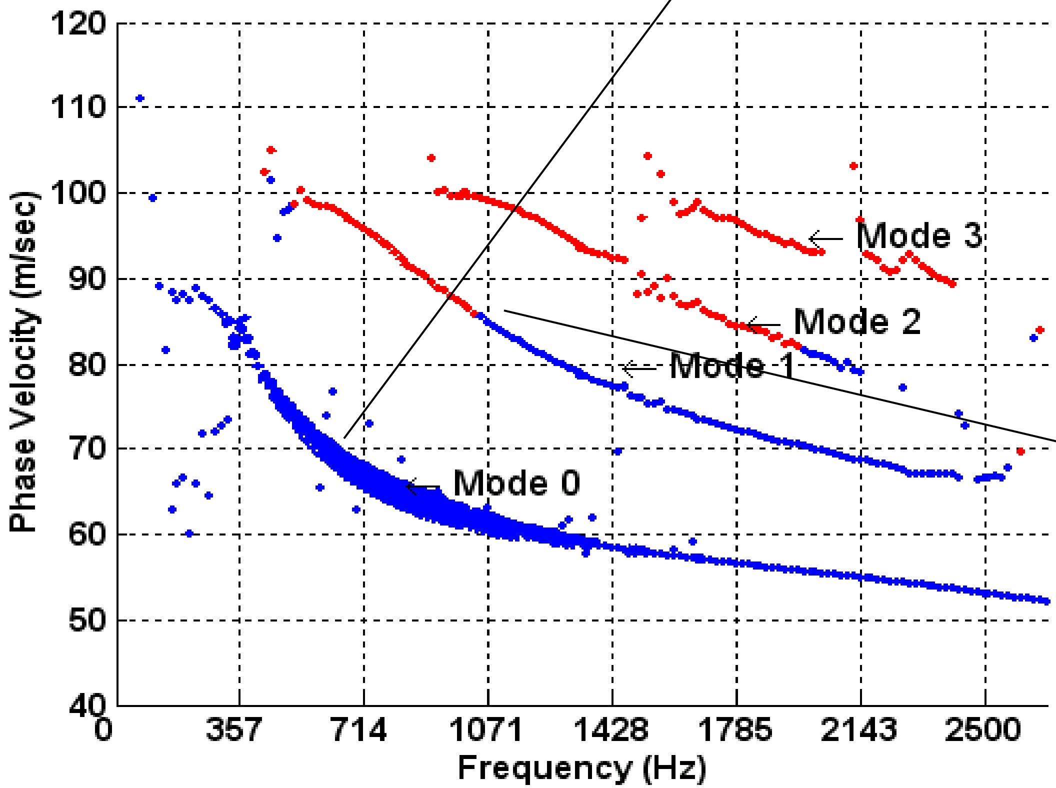

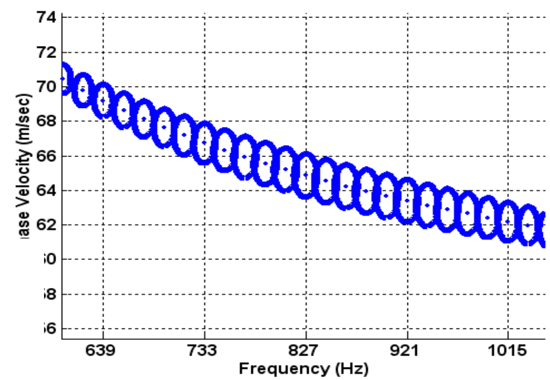

Rayleigh wave Polarization

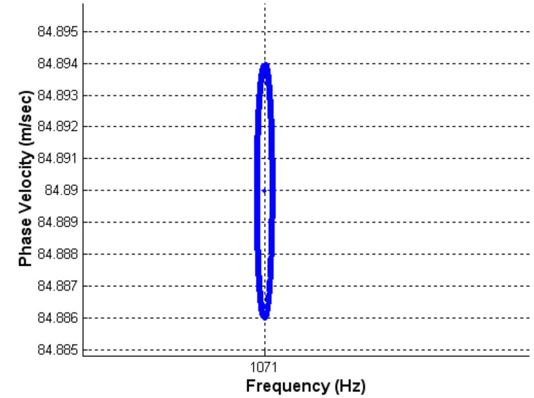

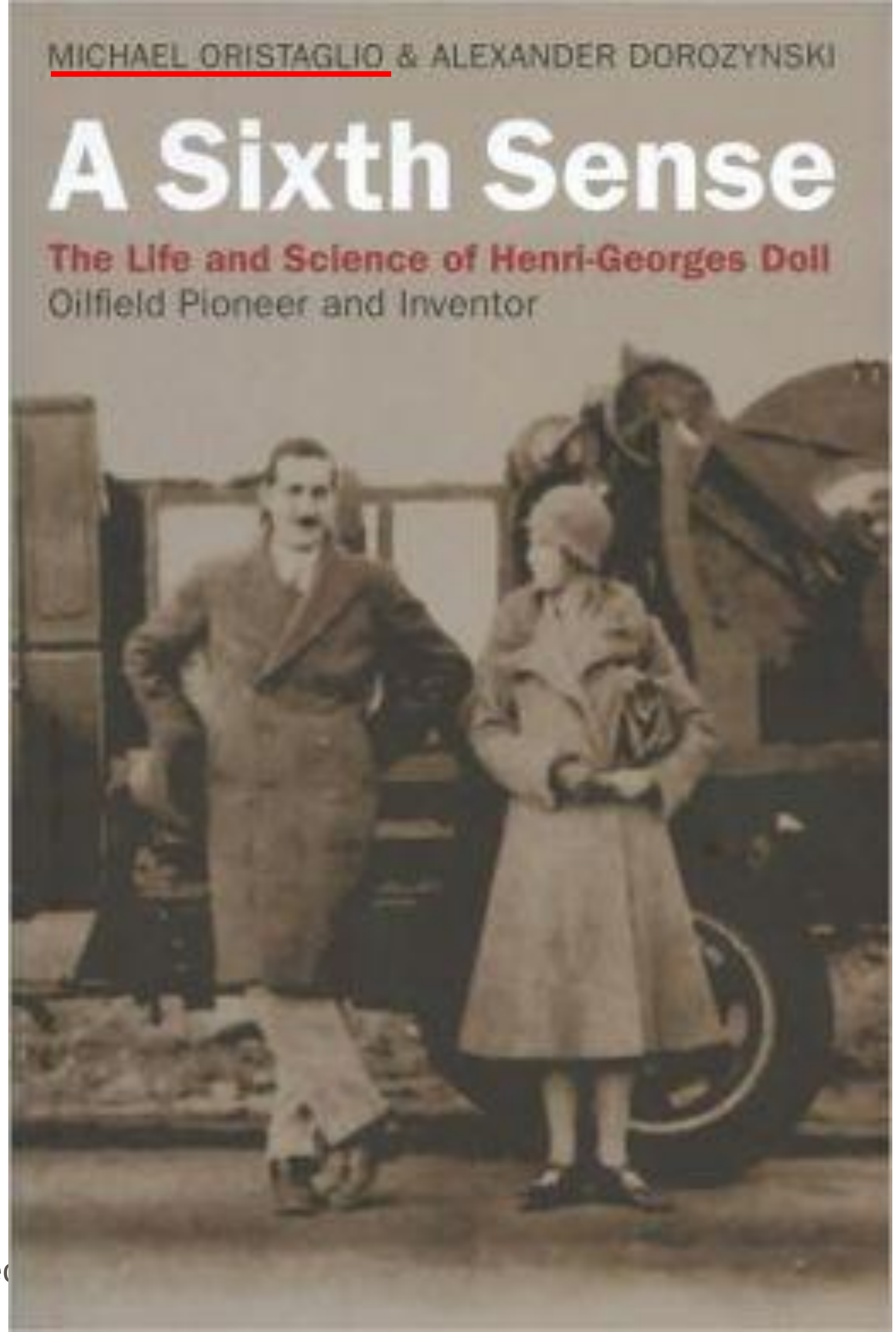
MICHAEL ORISTAGLIO & ALEXANDER DOROZYNSKI
A Sixth Sense
The Life and Science of Henri-Georges Doll
Oilfield Pioneer and Inventor

Henri Georges Doll (1902-1991)

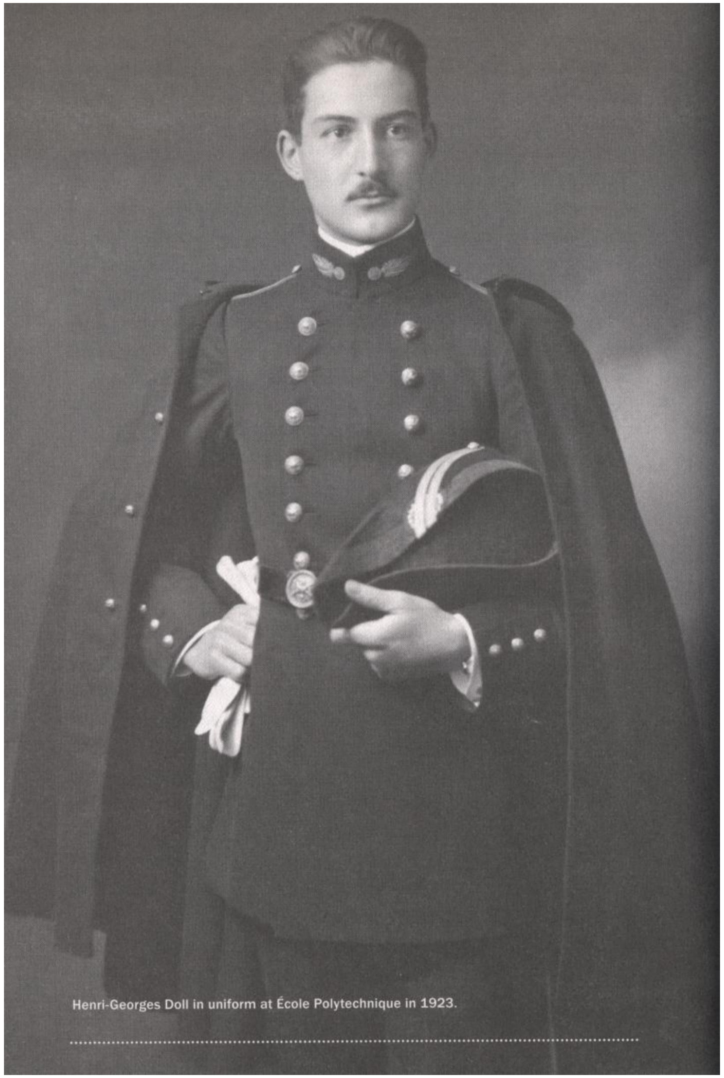

Landmine Detection

- 1877: Metal Detector Patent, Alexander Graham Bell
- 1941 patent: Jozef Kosacki, Polish signal officer stationed in Britain
  - ~5 kHz. Could be carried by soldier (14 kg)
- France and US wanted vehicle mounted system
  - 1940, Doll had an (EMI) prototype running in France
  - Fled France and escaped back to the US
    - Had lived and worked in Houston 1928—1938 as Schlumberger grew in US
- 1940: US started development of new mine detectors
  - Doll sets up EMR and spends 50% time during WWII
    - While continuing to serve as director at Schlumberger (SWSC)
  - 1943: won field trial vs. “Prairie Dog”
  - Delivered 505 systems by end of war

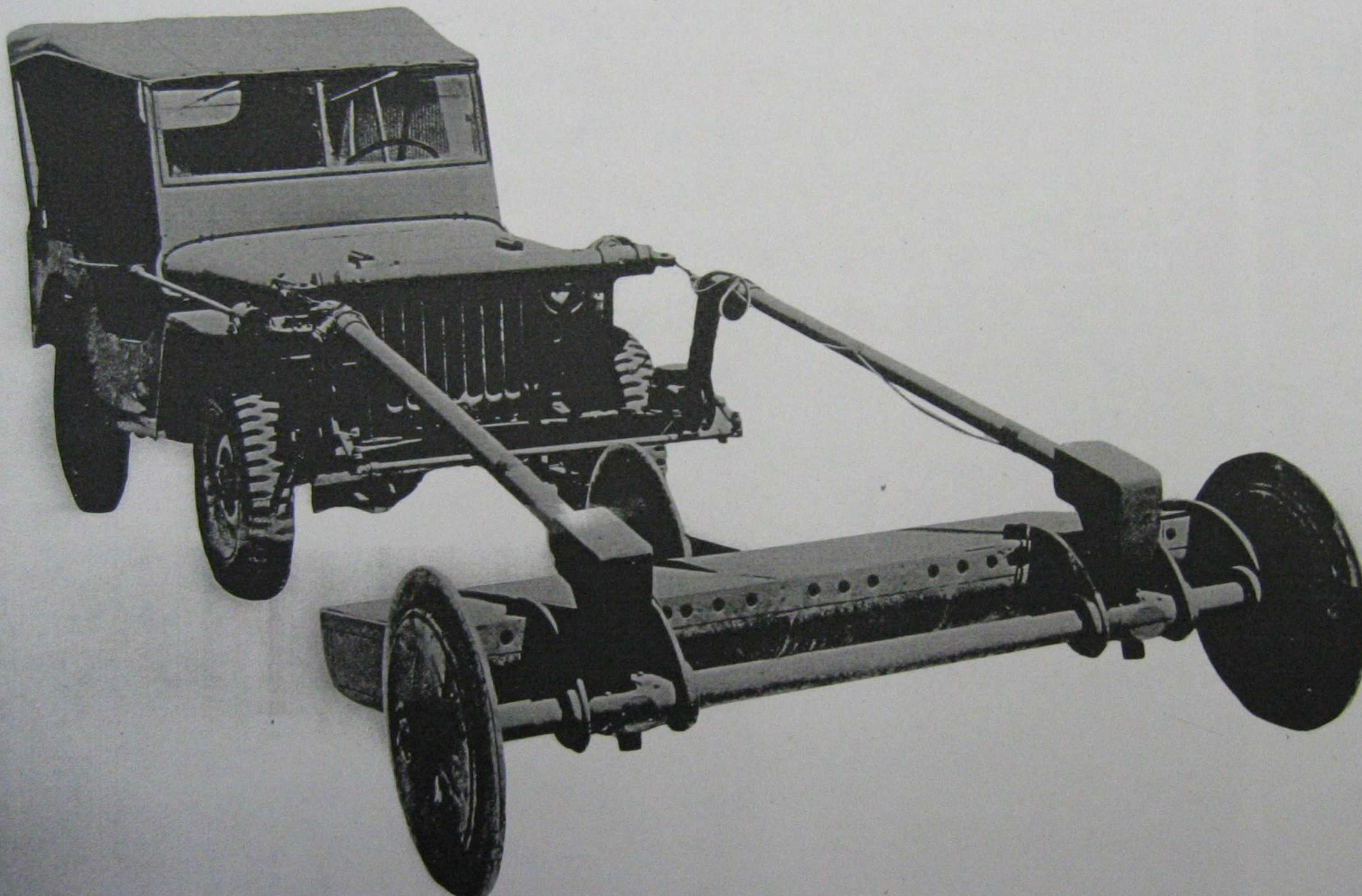

Vehicular Detector Set AN/VRS-2

Anecdotes

There were also lighter moments. As the orders from the army were filled, Jeeps with the mounting frame installed could be seen on the grounds of SWSC in Houston (where EMR was located). When neighbors asked about the curious-looking devices, the official explanation was that SWSC was developing a new plow for clearing snow from highways. It had not snowed in Houston in years.

During one trial of an early prototype, an army general visiting EMR insisted on riding in the vehicle. Doll, who was driving, asked the general to fasten his seat belt. The general just glared. Doll started driving. When the vehicle approached the first dummy mine, the automatic braking system engaged, bringing the Jeep to an abrupt stop. The general ended up on the hood.

Automatic Braking

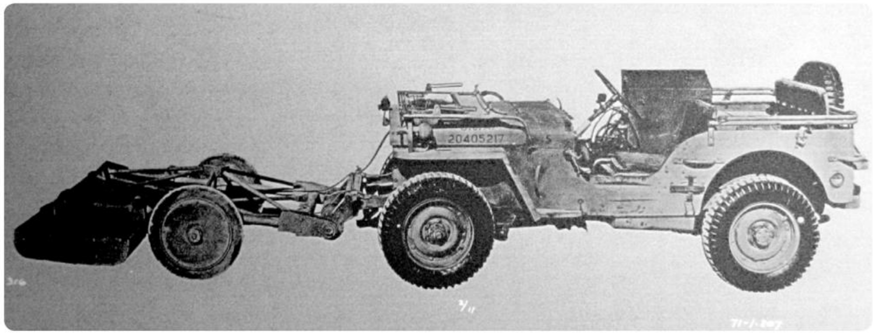

Jeep-mounted mine detector, AN/VRS-1, produced by EMR for The Engineer Board (*History of the Development of Electronic Equipment - I - Metallic Mine Detectors*, The Engineer Board, U.S. Army Corps of Engineers, 1945).

Henri Doll (1945)

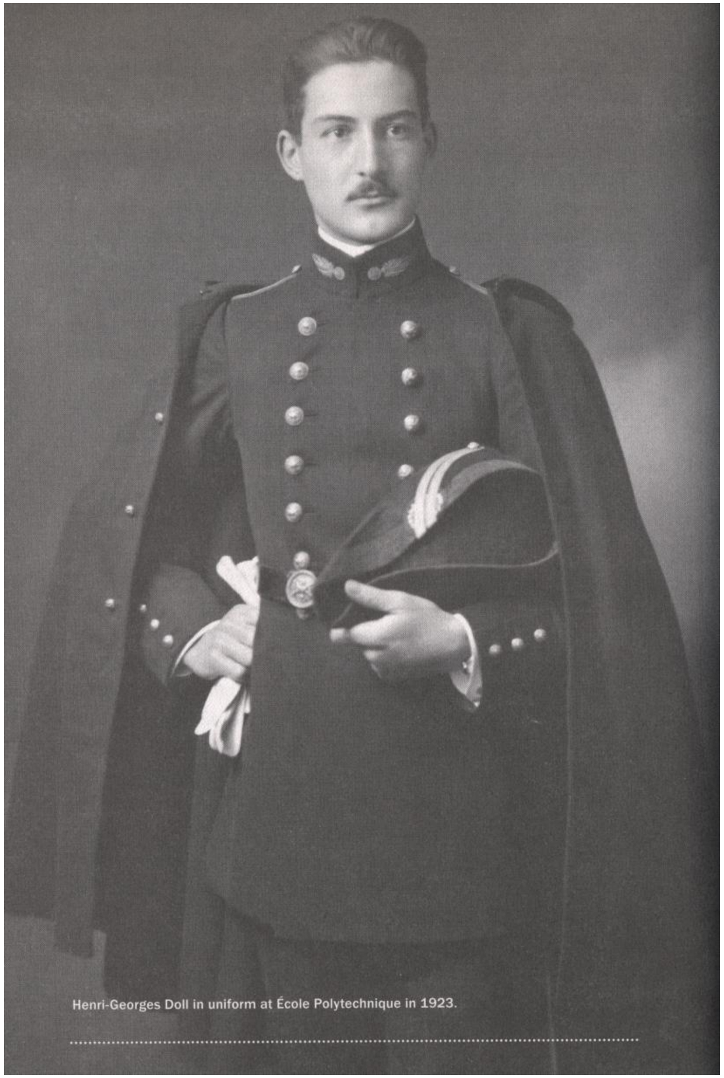

Henri-Georges Doll in uniform at École Polytechnique in 1923.

Henri-Georges Doll around 1945.

Ground Penetrating Radar

- GPR senses changes in the permittivity and conductivity of the subsurface
  - Advantages
    - Senses almost all targets of interest
    - Complements EMI (metal detectors)
    - Very fast
  - Disadvantages
    - Many sources of false alarms

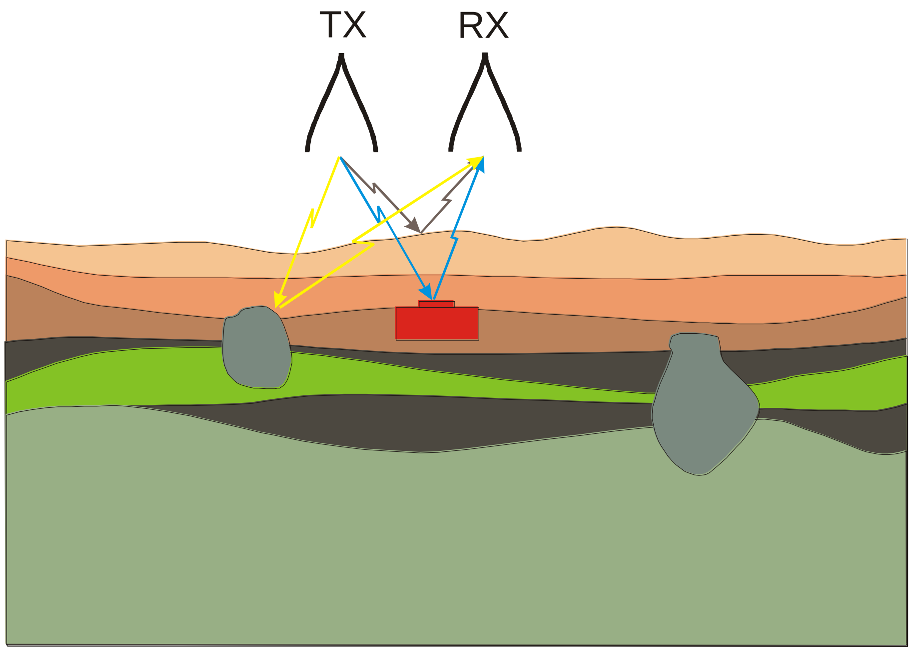

Sparsity-1

Signal Recovery from Undersampled Data

Incoherent Sampling Theorem (Candes and Romberg,2006)

- f is S-sparse in Ψ and $|f| = N$
- Select M measurements uniformly at random

$$M \gtrsim \mu^2(\Psi, \Phi) \cdot S \cdot \log N$$

- Solving

$$\hat{f} = \text{argmin} \, \|f\|_1 \qquad s.t. \quad y = \Phi \Psi f$$

  will reconstruct f exactly with overwhelming probability
- $\mu(\Psi, \Phi)$ is the coherence between Ψ and Φ

Sparsity-2

Robust Compressive Sensing

Signals are generally noisy. A realistic model for the measurements

$$y = \Phi x + z \quad z_k \;\; i.i.d \; N(0, \sigma^2)$$

Dantzig Selector (Candes and Tao)

- If the Restricted Isometry Property holds

$$\hat{f} = \operatorname{argmin} \|f\|_1 \quad s.t. \quad \|A^T(y - Af)\|_\infty < \epsilon_N \sigma.$$

- $A = \Phi\Psi$ and selecting $\epsilon_N = \sqrt{2 \log N}$ makes the true x feasible with high probability.

Dr. Ali Cafer Gurbuz: GPR-1

Ground Penetrating Radar (GPR)

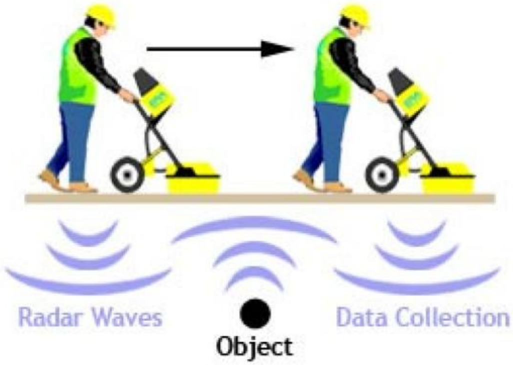

Impulse GPR

- Works in time domain
- Simpler design and low cost

Stepped Frequency GPR

- Greater measurement accuracy
- Operating frequency range can be adjusted
- Greater dynamic range and lower noise

Gurbuz: GPR-2

GPR Data Model

We assume that the received signal reflected from a point target at position p is a time delayed and scaled version of the transmitted signal s(t)

$$\zeta_i(t) = As(t - \tau_i(p))$$

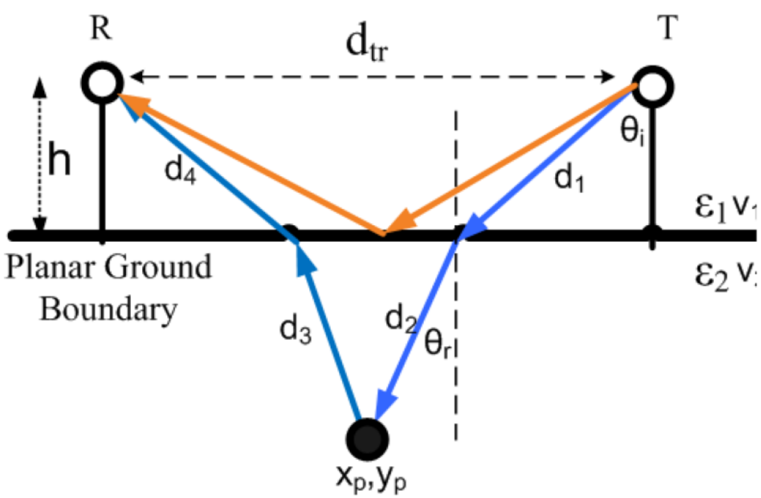

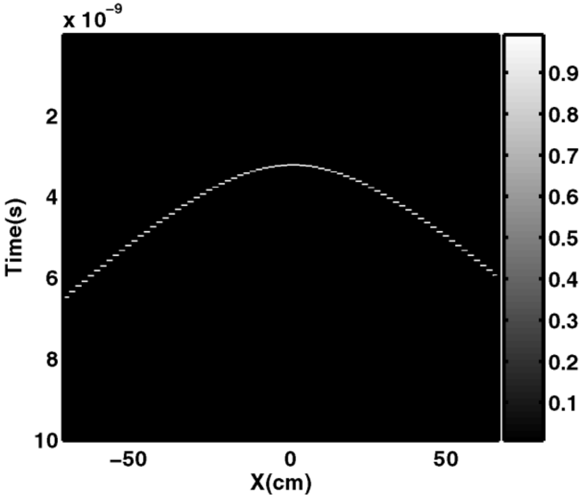

Gurbuz: GPR-3

Creating a dictionary for GPR Data

A discrete inverse operator can be created by discretizing the spatial domain target space and synthesizing the GPR model data for each discrete spatial position.

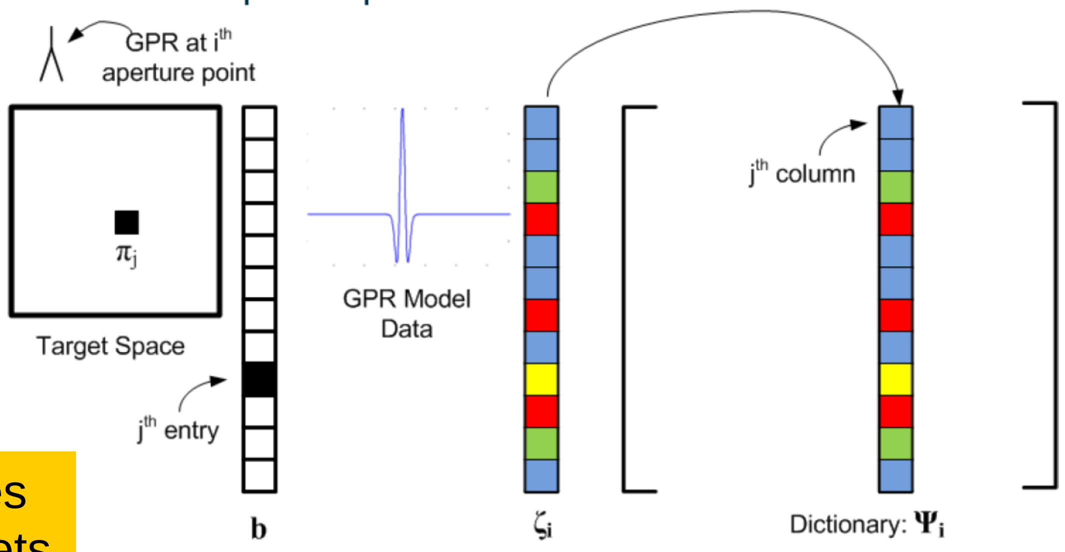

Enumerate responses from all possible targets

$$\zeta_i = \Psi_i b \qquad [\Psi_i]_j = \frac{s(t - \tau_i(\pi_j))}{\|s(t - \tau_i(\pi_j))\|_2}$$

Gurbuz: GPR-4

Frequency Domain Imaging - 1

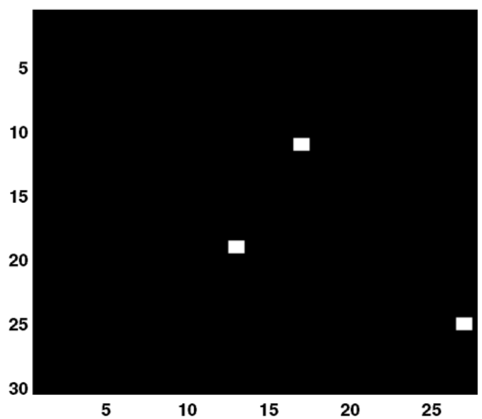

Target space

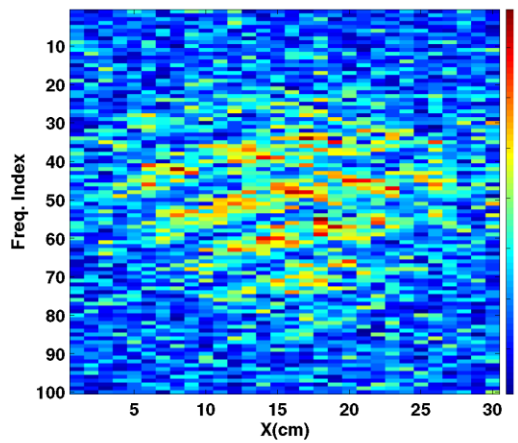

Space-frequency domain data (SNR $= 0\,\mathrm{dB}$)

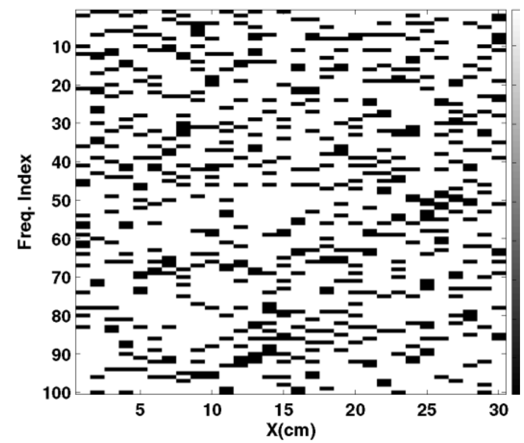

Measured Frequencies(black)

Gurbuz: GPR-5

Frequency Domain Imaging - 2

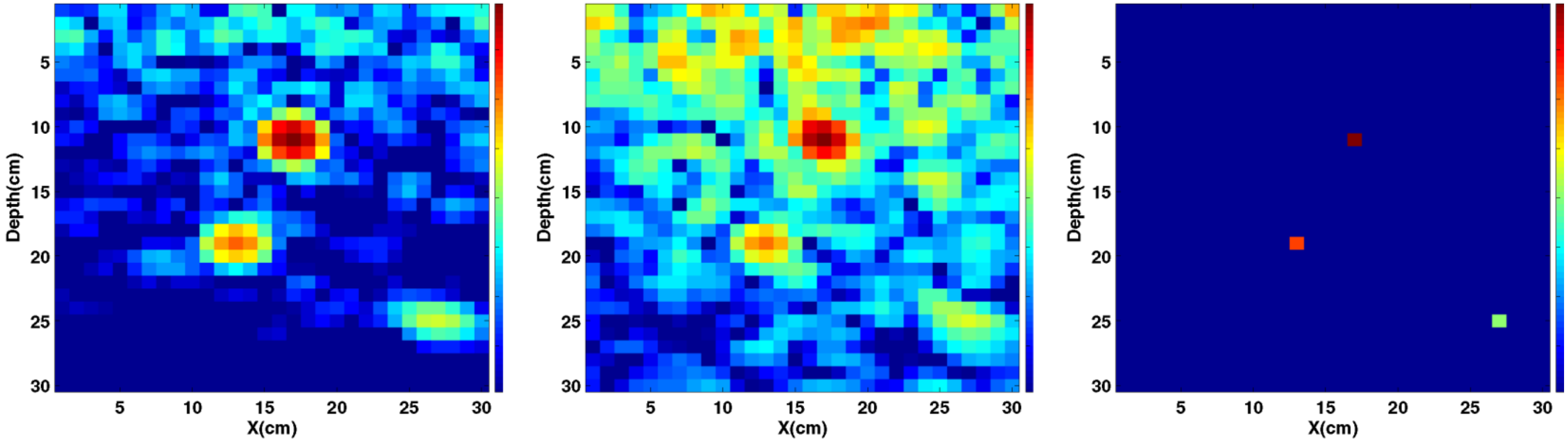

BP w/ all freq. data

BP w/ randomly selected data

CS w/ randomly selected data

Gurbuz: GPR-6

Random Spatial Sampling

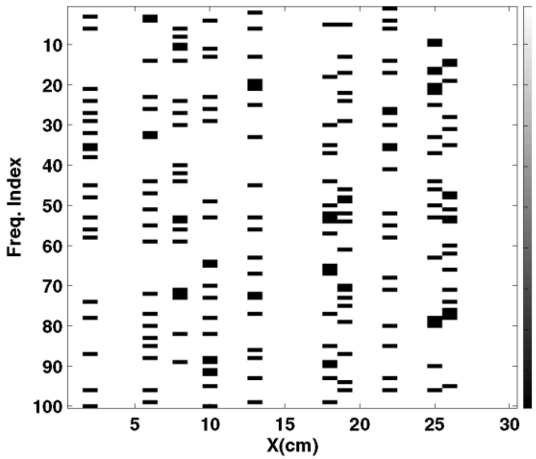

Measured
Space-frequency data

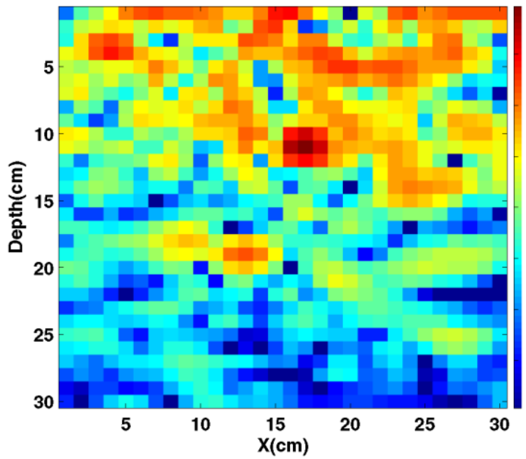

BP Result

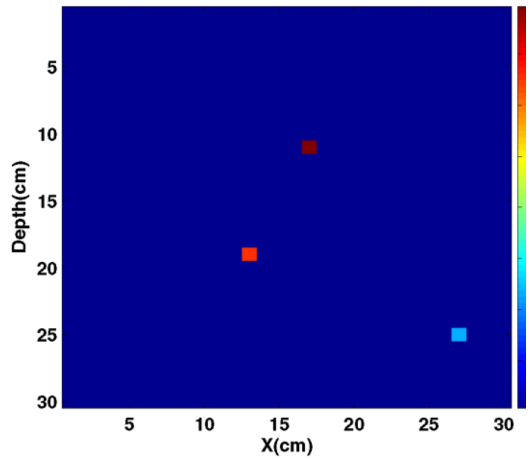

CS Result

Sparsity Concepts

- **<u>Enumerate</u>** all possible outcomes, and then **<u>pick</u>** the best one(s)

- Enumerate from a model
  - Sampling density of parameters
  - RIP ➔ more samples not necessarily better

- Pick the best, but not exhaustive search!
- Use L_1 optimization to pick the answer
  - Often group sparsity applies

EMI Sensing of Buried Targets

- EMI sensor will sense both
  - Magnetic susceptibility χ of the soil
  - Magnetic polarizability M of the targets
- Measure R but we want information about the subsurface
  - Target
    - Type
    - Spatial location
    - Spatial orientation
  - Soil
    - Magnetic Properties
    - Voids
    - Consistency
- How to get this information?
  - Very accurate measurements of R
  - Understand soil properties
  - Clever signal processing/inversion

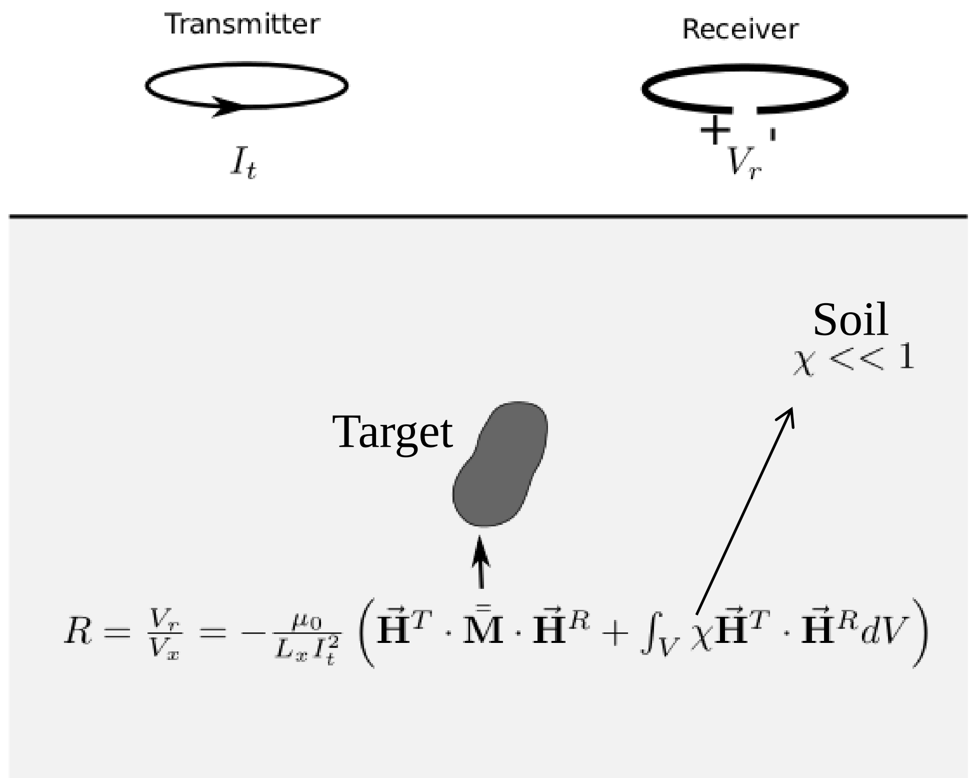

Sensor Development

- The hardware must quickly and accurately measure the response of a target to meet the goals
- Current systems
  - High dynamic range
  - Wide bandwidth: 300 Hz to 90 KHz
  - 21 logarithmically spaced frequencies
  - 30 to 90 Hz update rate
  - Uncoupled from the soil


Large Array EMI


Small Single EMI


Small Array EMI

EMI System

- Using a frequency-domain wideband EMI system
- $r_c(\omega, \boldsymbol{l}_s; \boldsymbol{l}_t, \boldsymbol{o}_t) = C\mathbf{g}_c^T(\boldsymbol{l}_s - \boldsymbol{l}_t)\boldsymbol{R}(\boldsymbol{o}_t)\mathbf{M}(\omega)\boldsymbol{R}^T(\boldsymbol{o}_t)\mathbf{f}(\boldsymbol{l}_s - \boldsymbol{l}_t)$
  - ω frequency
  - C constant defined by characteristics of the transmit and receive coils
  - $\mathbf{g}_c$ magnetic responses generated at the receive coil, c
  - $\mathbf{f}$ magnetic responses generated at the transmit coil
  - $\boldsymbol{R}$ rotation matrix
  - $\boldsymbol{o}_t$ 3D rotation angle of the target
  - $\boldsymbol{M}$ magnetization of the target

Enumerate responses from all possible targets ?

- If this response is built for every possible target, it scales as $\underline{\mathcal{O}(N^9)}$!
- $\boldsymbol{\Psi}_c^{\kappa}(\omega, \boldsymbol{l}_s; \boldsymbol{l}_t, \boldsymbol{o}_t) = \boldsymbol{g}_c^T(\boldsymbol{l}_s - \boldsymbol{l}_t)\boldsymbol{R}^T(\boldsymbol{o}_t)\boldsymbol{M}(\omega)\boldsymbol{R}(\boldsymbol{o}_t)\boldsymbol{f}(\boldsymbol{l}_s - \boldsymbol{l}_t)$

Sum of Dipoles Model

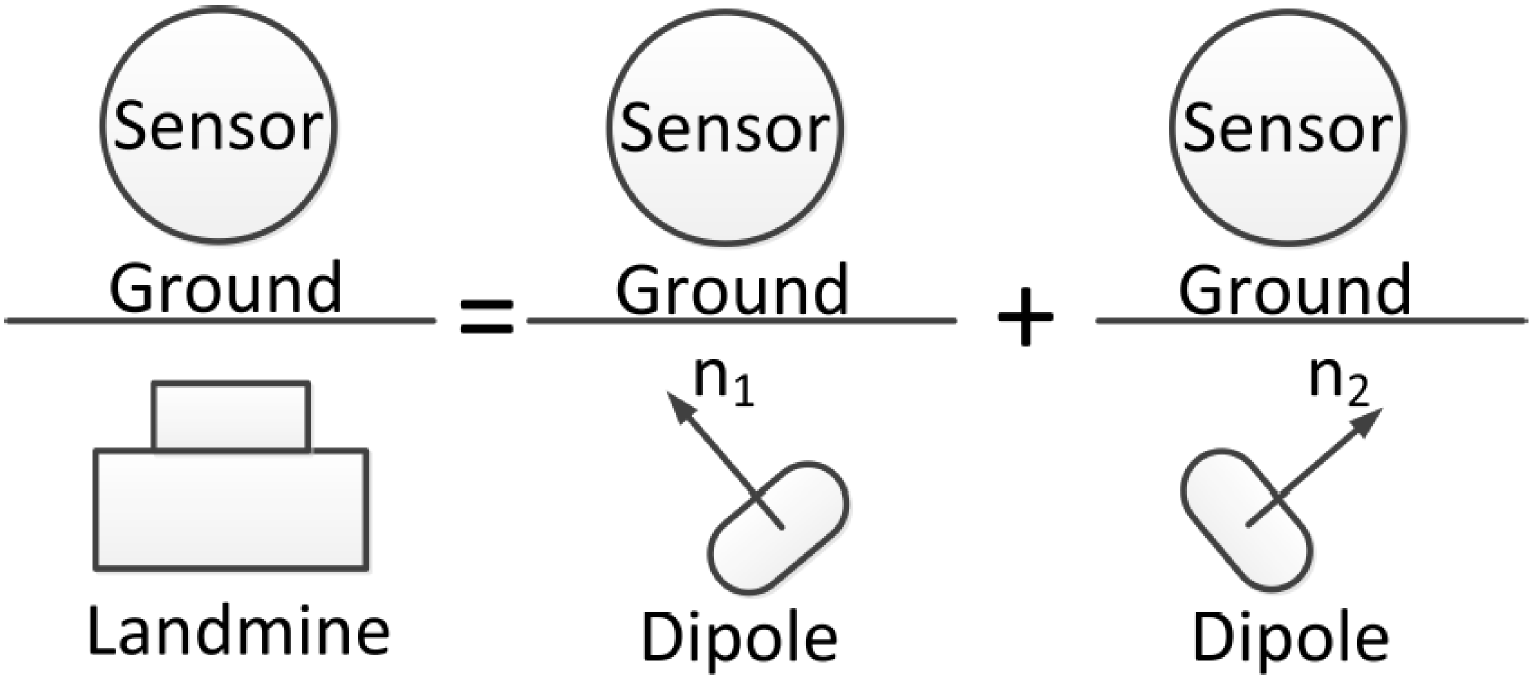

Magnetization

- Fully enumerated frequency model
  - $\boldsymbol{\Psi}_c^\kappa(\omega, \boldsymbol{l}_s; \boldsymbol{l}_t, \boldsymbol{o}_t) = \boldsymbol{g}_c^T(\boldsymbol{l}_s - \boldsymbol{l}_t)\boldsymbol{R}^T(\boldsymbol{o}_t)\boldsymbol{M}(\omega)\boldsymbol{R}(\boldsymbol{o}_t)\boldsymbol{f}(\boldsymbol{l}_s - \boldsymbol{l}_t)$
    1. $\boldsymbol{M}(\omega) = \sum_{k=0}^{N_\zeta} D_k p(\omega, \zeta_k)\boldsymbol{\Lambda}_k$
  - $\boldsymbol{\Psi}_c^\kappa(\omega, \boldsymbol{l}_s; \boldsymbol{l}_t, \boldsymbol{o}_t) = \sum_{k=0}^{N_\zeta} \upsilon_c^k(\boldsymbol{l}_s; \boldsymbol{l}_t, \boldsymbol{o}_t, \boldsymbol{\Lambda}_k) p_k(\omega, \zeta_k)$
- Now remove the frequency response and image the location and orientation dependent part
  - $\upsilon_c^k(\boldsymbol{l}_s; \boldsymbol{l}_t, \boldsymbol{o}_t) = \boldsymbol{g}_c^T(\boldsymbol{l}_s - \boldsymbol{l}_t)\boldsymbol{T}(\boldsymbol{o}_t, \boldsymbol{\Lambda}_k)\boldsymbol{f}(\boldsymbol{l}_s - \boldsymbol{l}_t)$
    1. $\boldsymbol{T}(\boldsymbol{o}_t, \boldsymbol{\Lambda}_k) = \boldsymbol{R}^T(\boldsymbol{o}_t)\boldsymbol{\Lambda}_k\boldsymbol{R}(\boldsymbol{o}_t) = \begin{bmatrix} t_1 & t_4 & t_6 \\ t_4 & t_2 & t_5 \\ t_6 & t_5 & t_3 \end{bmatrix}$
  - $\upsilon_c^k(\boldsymbol{l}_s; \boldsymbol{l}_t, \boldsymbol{o}_t) = \boldsymbol{\psi}_c^T(\boldsymbol{l}_s; \boldsymbol{l}_t)\boldsymbol{t}$

<u>Tensor</u> (6 params) instead of enumerating rotation angles

EMI Detection Algorithm

- A large, block-structured tensor $\boldsymbol{T}$ can be made which contains the approximated tensor at all N_{l_t} target locations

$$\boldsymbol{T} = \begin{bmatrix} \boldsymbol{T}_1(\boldsymbol{o}_t, \boldsymbol{\Lambda}_k) & 0 & 0 & 0 \\ 0 & \boldsymbol{T}_2(\boldsymbol{o}_t, \boldsymbol{\Lambda}_k) & 0 & 0 \\ & & \ddots & \vdots \\ 0 & 0 & & \\ 0 & 0 & \cdots & \boldsymbol{T}_{N_{\boldsymbol{l}_t}}(\boldsymbol{o}_t, \boldsymbol{\Lambda}_k) \end{bmatrix}$$

- $\boldsymbol{T}$ is low-rank, because the number of targets in a certain space will be sparse

<u>"Tensor Amplitude"</u>

EMI Detection Algorithm

- $\hat{\boldsymbol{T}}$ must be accurately extracted
- The properties of $\hat{\boldsymbol{T}}$ allow for the use of semidefinite programming (SDP)

$$\begin{aligned} \min \quad & \mathbf{tr}(\hat{\boldsymbol{T}}) \\ \text{s.t.} \quad & \hat{\boldsymbol{T}} \succeq 0 \\ & \| \mathbf{m} - \boldsymbol{\Psi}\hat{\mathbf{t}} \|_2 < \epsilon \end{aligned}$$

- Trace is a convex relaxation on rank minimization
- Requires an efficient solver

$$\hat{\boldsymbol{t}} = \begin{bmatrix} \boldsymbol{t}_1 \\ \boldsymbol{t}_2 \\ \vdots \\ \boldsymbol{t}_{6N_{l_t}} \end{bmatrix}$$

EMI Simulation

- Only two spatial dimensions, $\boldsymbol{l}_t = (y_t, z_t)$,
  - N_{y_t}=7 at 2cm spacing
  - N_{z_t}=8 at 1cm spacing
- Only two angles, $\boldsymbol{o}_t = (\alpha_t, \beta_t)$.
- Single target experiment
  - $\boldsymbol{l}_t = (0, 6.5)\,\mathrm{cm}$
  - $\boldsymbol{\Lambda} = \mathrm{diag}(0.5, 0, 1)$
  - $\boldsymbol{o}_t = (0^\circ, 22.5^\circ)$
  - Target is represented by a tensor

$$
\begin{aligned}
\boldsymbol{T} &= \begin{bmatrix} 0.57 & 0.00 & 0.17 \\ 0.00 & 0.00 & 0.00 \\ 0.17 & 0.00 & 0.92 \end{bmatrix} \\
&= \begin{bmatrix} 0.92 & 0.38 \\ 0 & 0 \\ -0.38 & 0.92 \end{bmatrix} \begin{bmatrix} 0.5 & 0 \\ 0 & 1 \end{bmatrix} \begin{bmatrix} 0.92 & 0.38 \\ 0 & 0 \\ -0.38 & 0.92 \end{bmatrix}^T
\end{aligned}
$$

EMI Simulation

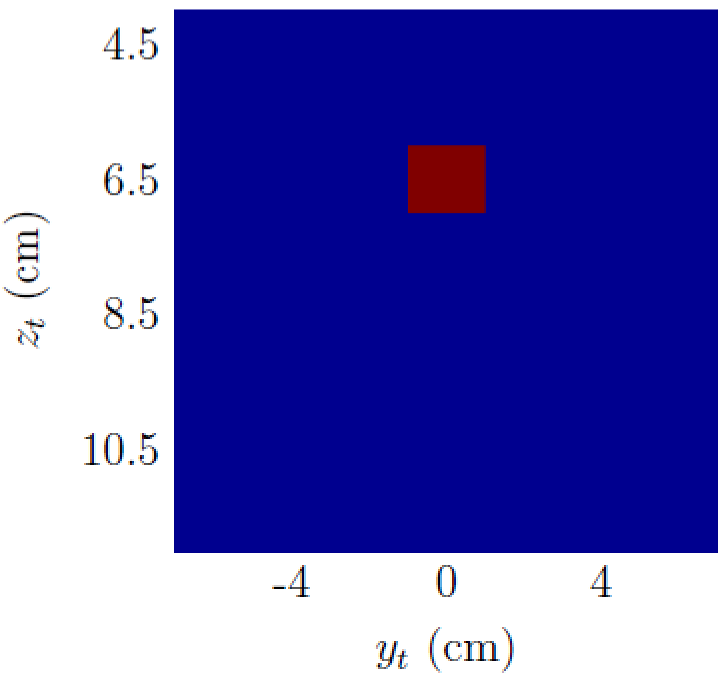

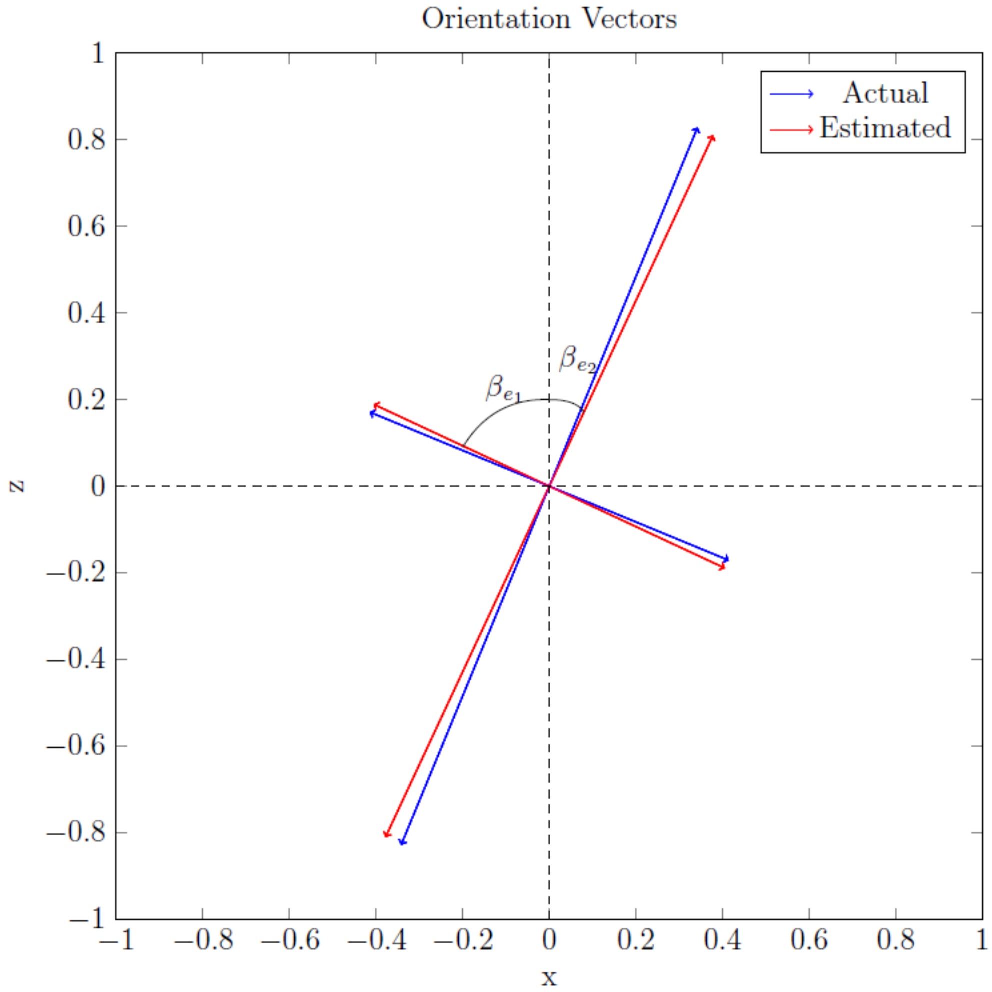

EMI Simulation

$$\hat{\boldsymbol{T}} = \begin{bmatrix} 0 & 0 & \cdots & 0 & \cdots & 0 \\ 0 & 0 & \cdots & 0 & \cdots & 0 \\ 0 & 0 & \ddots & \vdots & \ddots & \vdots \\ 0 & 0 & \cdots & \hat{\boldsymbol{T}}_{\boldsymbol{l}_t}(\boldsymbol{o}_t, \boldsymbol{\Lambda}) & \cdots & 0 \\ 0 & 0 & \ddots & \vdots & \ddots & \vdots \\ 0 & 0 & \cdots & 0 & \cdots & 0 \end{bmatrix}.$$

$$\hat{\boldsymbol{T}}_{\boldsymbol{l}_t}(\boldsymbol{o}_t, \boldsymbol{\Lambda}) = \begin{bmatrix} 0.57 & 0.01 & 0.20 \\ 0.01 & 0.00 & 0.00 \\ 0.20 & 0.00 & 0.89 \end{bmatrix}$$

$$= \begin{bmatrix} 0.90 & 0.42 \\ 0.03 & 0.00 \\ -0.42 & 0.90 \end{bmatrix} \begin{bmatrix} 0.48 & 0 \\ 0 & 1 \end{bmatrix} \begin{bmatrix} 0.90 & 0.42 \\ 0.03 & 0.00 \\ -0.42 & 0.90 \end{bmatrix}^T.$$

EMI Storage Requirements

- $N_{l_t} = 21{\times}31{\times}26 = 16926$
- $N_{l_s} = 201$
- Using full orientation enumeration with 5 degree resolution
  - $N_{o_t} = 18{\times}36{\times}36$
  - N_Λ is the number of types of symmetry, approx 3.
  - $3N_{l_s} \times N_{o_t} N_{l_t} N_\Lambda = 603{\times}(1{\times}109)$: approx 900 Gbytes
- Tensor representation storage
  - $3N_{l_s} \times 6N_{l_t} = 603{\times}(1{\times}105)$: approx 250 Mbytes

Sparsity-Aware Parameter Estimation for Multiple Microseismic Events

Hadi Jamali-Rad

h.jamalirad@tudelft.nl

Circuits and Systems (CAS) Group – Delft Univ. of Tech. (TU Delft)

Georgia Tech
April 2014

Acknowledgement:
Shell Global Solution B.V.
Rijswijk, The Netherlands

Prof. Geert Leus (IEEE Fellow)

PhD advisor from CAS group

Background and Objectives

- ❑ <u>Hydraulic Fracturing?</u>
  - ❖ Low permeability
  - ❖ Stimulation by creating <u>fractures</u>
  - ❖ Water & sand to stop collapse

  Fracture = Microseismic source

- ❑ <u>Why do we want to know?</u>
  - ❖ Productivity
  - ❖ Opening, shearing, effectiveness
  - ❖ Event detection and sync.

- ❑ <u>What do we want to know?</u>
  - ❖ Hypocenter
  - ❖ Moment tensors
  - ❖ Origin time

- ❑ <u>What do we measure?</u>
  - ❖ Displacement traces
  - ❖ Geophone arrays

- ❑ <u>Our Goal?</u>
  - ✓ Fast & accurate recovery of source parameters

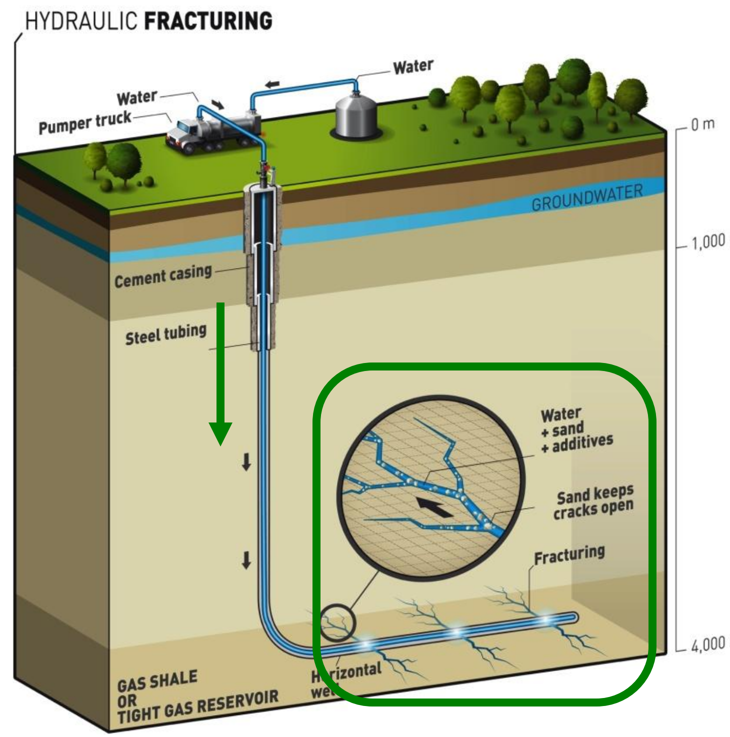

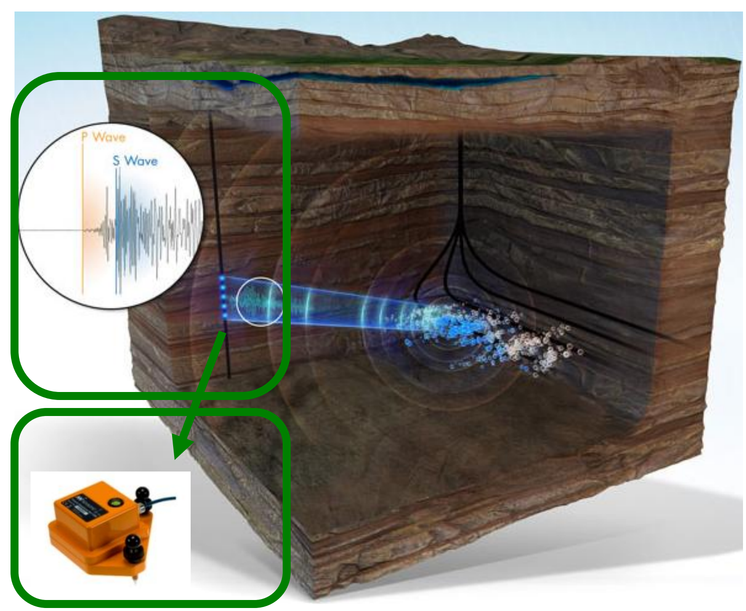

The Basic Idea

- ***What is missed? Does it help?***
  - **SPARSITY (in spatial domain)**
  - **Incorporate in the model: Sparsity-Aware!**

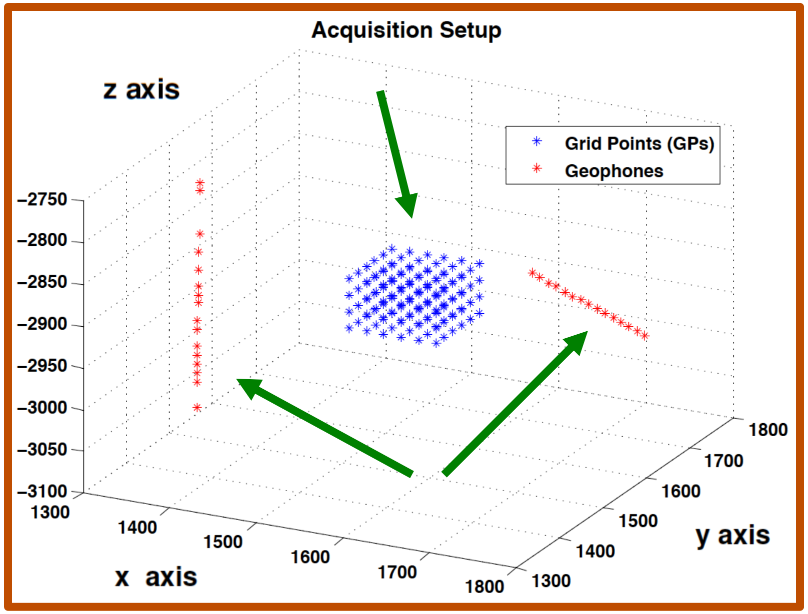

Green's Functions: Ray Tracing

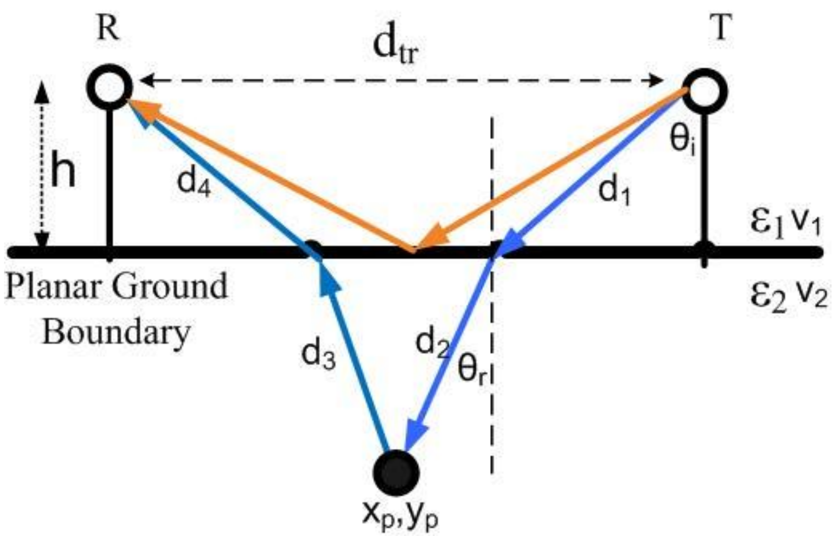

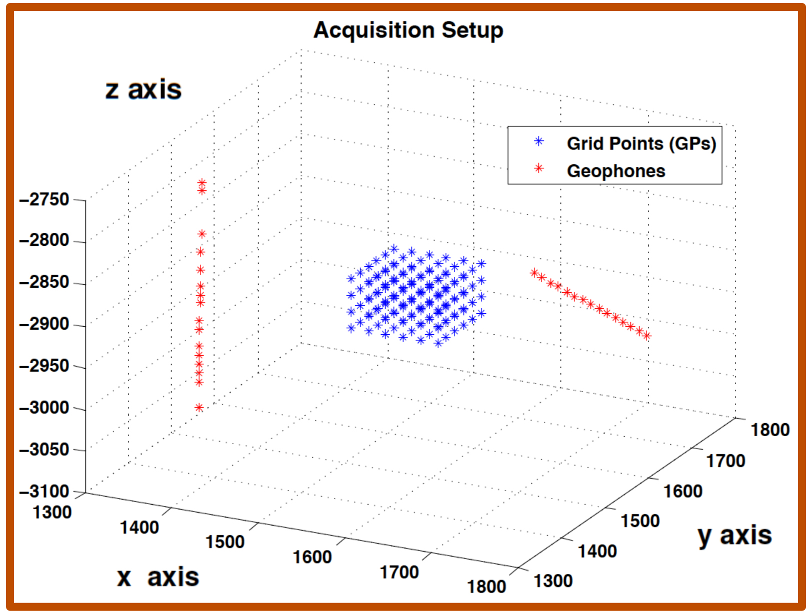

First Approach

Preliminaries

❑ **Moment tensor source model**

$$\mathbf{M}(t) = \mathbf{M}s(t)$$

$$\mathbf{M} = \begin{bmatrix} m_{xx} & m_{xy} & m_{xz} \\ & m_{yy} & m_{yz} \\ & & m_{zz} \end{bmatrix}$$

❑ **Displacement received from a tensor source**

$$\begin{aligned} \mathbf{u}_n(\mathbf{x}, t) &= \sum_{pq} \mathbf{M}_{pq}(t) * \frac{\partial}{\partial \boldsymbol{\zeta}_q} \mathbf{G}_{np}(\mathbf{x},\ \boldsymbol{\zeta},\ t,\ \tau) \\ &= \sum_{pq} \mathbf{M}_{pq}\, s(t) * \frac{\partial}{\partial \boldsymbol{\zeta}_q} \mathbf{G}_{np}(\mathbf{x},\ \boldsymbol{\zeta},\ t,\ \tau) \end{aligned}$$

Second Approach

A practical constraint

The validity and accuracy of the proposed approach relies on the knowledge of the *source time function*:

$$\underbrace{\begin{bmatrix} \mathbf{u}_x(\mathbf{x},t) \\ \mathbf{u}_y(\mathbf{x},t) \\ \mathbf{u}_z(\mathbf{x},t) \end{bmatrix}}_{\mathbf{u}(\mathbf{x},t)} = \underbrace{\begin{bmatrix} \boxed{s(t)} * \frac{\partial}{\partial\zeta_x}\mathbf{G}_{xx} & s(t) * \frac{\partial}{\partial\zeta_y}\mathbf{G}_{xx} & \cdots & s(t) * \frac{\partial}{\partial\zeta_z}\mathbf{G}_{xz} \\ s(t) * \frac{\partial}{\partial\zeta_x}\mathbf{G}_{yx} & s(t) * \frac{\partial}{\partial\zeta_y}\mathbf{G}_{yx} & \cdots & s(t) * \frac{\partial}{\partial\zeta_z}\mathbf{G}_{yz} \\ s(t) * \frac{\partial}{\partial\zeta_x}\mathbf{G}_{zx} & s(t) * \frac{\partial}{\partial\zeta_y}\mathbf{G}_{zx} & \cdots & s(t) * \frac{\partial}{\partial\zeta_z}\mathbf{G}_{zz} \end{bmatrix}}_{\mathbf{\Psi}(\mathbf{x},\ \zeta,\ t,\ \tau)} \underbrace{\begin{bmatrix} m_{xx} \\ m_{xy} \\ \vdots \\ m_{zz} \end{bmatrix}}_{\mathbf{m}(\zeta)}$$

- ❑ **Is there a way to eliminate this *crucial need*?**

✓ **A sparsity-aware framework *blind* to *s(t)*!**

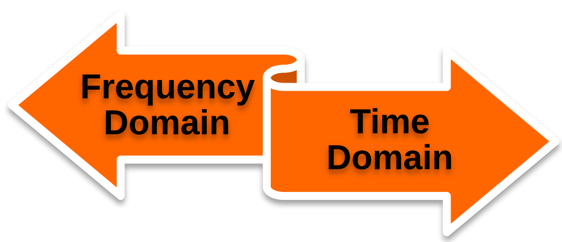

Second Approach

Modeling: Freq.-Domain

$$\tilde{\mathbf{u}}_n(\mathbf{x},\omega) = \sum_{pq} \mathbf{M}_{pq} \frac{\partial}{\partial \zeta_q} \tilde{\mathbf{G}}_{np}(\mathbf{x},\ \zeta,\ \omega)\, \tilde{s}(\omega)\, e^{j\omega\tau}$$

$$\tilde{u}_n(\mathbf{x},\omega_q) = \sum_{pq} \mathbf{M}_{pq} \frac{\partial}{\partial \zeta_q} \tilde{\mathbf{G}}_{np}(\mathbf{x},\ \zeta,\ \omega_q)\, \tilde{s}(\omega_q)\, e^{j\omega_q\tau}$$

3 × 1

$$\underbrace{\begin{bmatrix} \tilde{u}_x(\mathbf{x},\omega_q) \\ \tilde{u}_y(\mathbf{x},\omega_q) \\ \tilde{u}_z(\mathbf{x},\omega_q) \end{bmatrix}}_{\tilde{\mathbf{u}}(\mathbf{x},\omega_q)} = \underbrace{\boxed{\tilde{s}(\omega_q)} \begin{bmatrix} \frac{\partial}{\partial\zeta_x}\tilde{\mathbf{G}}_{xx} & \frac{\partial}{\partial\zeta_y}\tilde{\mathbf{G}}_{xx} & \cdots & \frac{\partial}{\partial\zeta_z}\tilde{\mathbf{G}}_{xz} \\ \frac{\partial}{\partial\zeta_x}\tilde{\mathbf{G}}_{yx} & \frac{\partial}{\partial\zeta_y}\tilde{\mathbf{G}}_{yx} & \cdots & \frac{\partial}{\partial\zeta_z}\tilde{\mathbf{G}}_{yz} \\ \frac{\partial}{\partial\zeta_x}\tilde{\mathbf{G}}_{zx} & \frac{\partial}{\partial\zeta_y}\tilde{\mathbf{G}}_{zx} & \cdots & \frac{\partial}{\partial\zeta_z}\tilde{\mathbf{G}}_{zz} \end{bmatrix}}_{\tilde{\boldsymbol{\Psi}}(\mathbf{x},\ \boldsymbol{\zeta},\ \omega_q)} \underbrace{\begin{bmatrix} m_{xx} \\ m_{xy} \\ \vdots \\ m_{zz} \end{bmatrix} \boxed{e^{j\omega_q\tau}}}_{\tilde{\mathbf{m}}(\boldsymbol{\zeta},\omega_q,\tau)}$$

$$\begin{aligned} \tilde{\mathbf{u}}(\omega_q) &= [\mathbf{u}_1(\omega_q)^T, \cdots \mathbf{u}_M(\omega_q)^T]^T \\ &= \sum_{k=1}^{K} \underbrace{[\tilde{\boldsymbol{\Psi}}_1(\boldsymbol{\zeta}_k,\omega_q)^T, \tilde{\boldsymbol{\Psi}}_2(\boldsymbol{\zeta}_k,\omega_q)^T, \cdots, \tilde{\boldsymbol{\Psi}}_M(\boldsymbol{\zeta}_k,\omega_q)^T]^T}_{\tilde{\boldsymbol{\Psi}}(\boldsymbol{\zeta}_k,\omega_q)} \tilde{\mathbf{m}}(\boldsymbol{\zeta}_k,\omega_q,\tau_k) \end{aligned}$$

3 *M* × 1

Second Approach

A novel estimator

$$\tilde{\mathbf{u}}(\omega_q) = \underbrace{\left[\tilde{\boldsymbol{\Psi}}_1(\omega_q), \tilde{\boldsymbol{\Psi}}_2(\omega_q), \cdots, \tilde{\boldsymbol{\Psi}}_N(\omega_q)\right]}_{\tilde{\boldsymbol{\Psi}}(\omega_q)} \tilde{\mathbf{m}}(\omega_q)$$

3 M × 6N

$$\tilde{\mathbf{m}}(\omega_q) = [\tilde{\mathbf{m}}_1(\omega_q)^T, \tilde{\mathbf{m}}_2(\omega_q)^T, \cdots, \tilde{\mathbf{m}}_N(\omega_q)^T]^T$$

- ❑ **How can we handle N_f dictionaries and measurement vectors?**

A novel estimator:

- ✓ **Take the *specific group structure* into account**
- ✓ **Take the *common sparsity support* in different frequencies into account**

$$\hat{\boldsymbol{\Theta}}_{\text{MG-LASSO}} = \arg\min_{\boldsymbol{\Theta}} \sum_{q=1}^{N_f} \|\tilde{\mathbf{u}}(\omega_q) - \tilde{\boldsymbol{\Psi}}(\omega_q)[\boldsymbol{\Theta}]_{:,q}\|_2^2 + \lambda \sum_{n=1}^{N} \|[\boldsymbol{\Theta}]_{6(n-1)+1:6n\,,:}\|_2$$

Accuracy (LS part per freq) **Group sparsity**

$$\boldsymbol{\Theta} = [\tilde{\mathbf{m}}(\omega_1), \cdots, \tilde{\mathbf{m}}(\omega_{N_f})]$$

Regularization

Recap

- 3-axis sensors everywhere
- Tensor representation
  - Formidable Computation
- Sparse Representations
  - Simplify Models
- Compressive Sensing
  - Simpler Acquisition